List of Publications and Patent

Preprint:

- **Chattopadhyay A**, Jagdish S, Karhale AK, Ramteke N, Zaib A, **Nandi D**. Interferon-γ lowers tumour growth by increasing glycolysis and lactate production in a nitric oxide-dependent manner: implications for cancer immunotherapy. bioRxiv. 2023:2023-07.

Publications:

- **Chattopadhyay A**, Joseph JP, Jagdish S, Chaudhuri S, Ramteke NS, Karhale AK, Waturuocha U, Saini DK, **Nandi D**. High throughput screening identifies auranofin and pentamidine as potent compounds that lower IFN-γ-induced Nitric Oxide and inflammatory responses in mice: DSS-induced colitis and Salmonella Typhimurium-induced sepsis. International Immunopharmacology. 2023 Sep 1;122:110569.

- **Chattopadhyay A**, Joseph JP, Shyam S, **Nandi D**. Characterizing Salmonella Typhimurium-induced Septic Peritonitis in Mice. JoVE (Journal of Visualized Experiments). 2022 Jul 29(185):e63695.

- Rananaware SR, Pathak S, Chakraborty S, Bisen RY, **Chattopadhyay A**, **Nandi D**. Autoimmune-prone lpr mice exhibit a prolonged but lethal infection with an attenuated Salmonella Typhimurium strain. Microbial Pathogenesis. 2021 Jan 1;150:104684.

- **Nandi D**, Pathak S, Verma T, Singh M, **Chattopadhyay A**, Thakur S, Raghavan A, Gokhroo A, Vijayamahantesh. T cell costimulation, checkpoint inhibitors and anti-tumor therapy. Journal of biosciences. 2020 Dec;45:1-36.

- Yadav S, Verma T, **Chattopadhyay A**, **Nandi D**. Factors affecting the pathophysiology of sepsis, an inflammatory disorder: Key roles of oxidative and nitrosative stress. Indian Journal of Inflammation Research. 2019;3(1):2.

Patent:

- **Indian Provisional Patent Application No.: 202341039378**

  Filing date: 08/06/2023

  Title: “MODEL(S) FOR IDENTIFICATION OF ANTIINFLAMMATORY COMPOUNDS AND COMPOUNDS DETERMINED THEREFROM”

  Applicants: INDIAN INSTITUTE OF SCIENCE

  Student investigator: **Avik Chattopadhyay (BC, IISc)**

  Principal investigators: **Prof. Deepak Saini (DBG, IISc)**, **Prof. Dipankar Nandi (BC, IISc)**

Copies of Two Publications are presented in the following pages.

International Immunopharmacology 122 (2023) 110569

Contents lists available at ScienceDirect

International Immunopharmacology

journal homepage: www.elsevier.com/locate/intimp

High throughput screening identifies auranofin and pentamidine as potent compounds that lower IFN-γ-induced Nitric Oxide and inflammatory responses in mice: DSS-induced colitis and *Salmonella* Typhimurium-induced sepsis

Avik Chattopadhyay [a], Joel P. Joseph [b], Sirisha Jagdish [a], Somak Chaudhuri [a], Nikita S. Ramteke [a], Aagosh Kishore Karhale [a], Uchenna Waturuocha [c], Deepak Kumar Saini [b,c], Dipankar Nandi [a,*]

[a] *Department of Biochemistry, Indian Institute of Science, Bangalore 560012, India*
[b] *Centre for BioSystems Science and Engineering, Indian Institute of Science, Bangalore 560012, India*
[c] *Department of Developmental Biology and Genetics, Indian Institute of Science, Bangalore 560012, India*

ARTICLE INFO

Keywords:
Colitis
Interferon-gamma
LOPAC®[1280]
Nitric Oxide
Peritonitis
Sepsis

ABSTRACT

Interferon-gamma (IFN-γ) is a type II interferon produced primarily by T cells and natural killer cells. IFN-γ induces the expression of inducible nitric oxide synthase (NOS2) to catalyze Nitric Oxide (NO) production in various immune and non-immune cells. Excessive IFN-γ-activated NO production is implicated in several inflammatory diseases, including peritonitis and inflammatory bowel diseases. In this study, we screened the LOPAC®[1280] library *in vitro* on the H6 mouse hepatoma cell line to identify novel non-steroidal small molecule inhibitors of IFN-γ-induced NO production. Compounds with the highest inhibitory activity were validated, which led to identifying the lead compounds: pentamidine, azithromycin, rolipram, and auranofin. Auranofin was the most potent compound determined based on IC_{50} and goodness of fit analyses. Mechanistic investigations revealed that majority of the lead compounds suppress the IFN-γ-induced transcription of *Nos2* without negatively affecting NO-independent processes, such as the IFN-γ-induced transcription of *Irf1*, *Socs1* and MHC class 1 surface expression. However, all four compounds lower IFN-γ-induced reactive oxygen species amounts. In addition, auranofin significantly reduced IFN-γ-mediated NO and IL6 production in resident as well as thioglycolate-elicited peritoneal macrophages (PMs). Finally, *in vivo* testing of the lead compounds in the preclinical DSS-induced ulcerative colitis mice model revealed pentamidine and auranofin to be the most potent and protective lead compounds. Also, pentamidine and auranofin greatly increase the survival of mice in another inflammatory model: *Salmonella* Typhimurium-induced sepsis. Overall, this study identifies novel anti-inflammatory compounds targeting IFN-γ-induced NO-dependent processes to alleviate two distinct inflammatory models of disease.

1. Introduction

Interferons, originally discovered to interfere in the process of viral replication, modulate a multitude of biological functions and is involved in disease pathogenesis. They are classified as Type I, Type II and Type II IFNs. Interferon-gamma (IFN-γ) is the only type II IFN structurally unrelated to Type I IFNs. The cellular sources of IFN-γ include $CD4^+$ T helper cell type 1 (Th1) lymphocytes, $CD8^+$ cytotoxic lymphocytes, Natural Killer cells, etc. The binding of IFN-γ to its receptor results in the receptor's phosphorylation by JAK, enabling the receptor's Src homology 2 (SH2) domains to bind to STAT1 for subsequent activation. Phosphorylated STAT1 monomers form a homodimer known as Gamma-

Abbreviations: DMEM-HG, Dulbecco's modified minimal essential medium-High Glucose; DSS, Dextran Sodium Sulfate; IBD, Inflammatory Bowel Disease; IFN-γ, Interferon-gamma; IL, Interleukin; IRF, Interferon regulatory factor; LNMA, NG-Methyl-L-arginine acetate salt; LOPAC, Library of Pharmacologically Active Compounds; NO, Nitric Oxide; NOS, Nitric Oxide Synthase; PM, Peritoneal Macrophage; TNF, Tumor Necrosis Factor.

* Corresponding author.
E-mail address: nandi@iisc.ac.in (D. Nandi).

https://doi.org/10.1016/j.intimp.2023.110569
Received 2 May 2023; Received in revised form 8 June 2023; Accepted 23 June 2023

activated factor (GAF), which gets translocated into the nucleus. GAF binds to the Gamma-activating sequence (GAS) to activate the genes responsible for the primary transcriptional response *(Irf1, Irf9)*. One of the targets of GAF is interferon regulatory factor 1 (IRF1), a transcription factor that binds on Interferon stimulated response elements (*Isre*) and initiates the secondary transcriptional program of its target genes (*Gbp1*, *Psmb10*). The expression of NOS2 catalyzing the production of Nitric Oxide (NO) is one of the key markers in IFN-γ signaling in different cell types, including macrophages and tumors [1,2].

NO is a gaseous free radical that mediates intra- and inter-cellular communication to perform essential roles in various physiological processes. NO is produced by a family of enzymes called nitric oxide synthases (NOS). There are three isoforms of NOS: neuronal NOS (nNOS or NOS1), inducible NOS (iNOS or NOS2), and endothelial NOS (eNOS or NOS3). All three isoforms of NOS produce NO by converting the amino acid L-arginine to L-citrulline using oxygen and NADPH as cofactors. *Nos2* is primarily expressed in immune cells such as macrophages and is induced by pro-inflammatory cytokines such as IFN-γ and bacterial products such as Lipopolysaccharide (LPS) [3]. The catalytic activity of NOS isoforms is regulated by various mechanisms, including calcium/calmodulin binding, phosphorylation, and the availability of substrate and cofactors. However, the expression of *Nos2* depends on intracellular calcium, but not the catalytic activity of NOS2, facilitating faster action than other NOS isoforms. NO mediates pleiotropic downstream effects and regulates the outcomes of the IFN-γ signaling pathway [4].

IFN-γ and other cytokines are involved in many inflammatory disease progression and pathogenesis. For instance, in tuberculosis, the IFN-γ-activation of Mycobacterium-infected murine macrophages effectively clears off the infection. These beneficial effects are attributed to the IFN-γ-mediated NO production, following NO-dependent transcriptional activation of antimicrobial pathways, direct microbicidal action, and host cell apoptosis [5,6]. The IFN-γ-NO axis also ameliorates other infectious diseases such as leishmaniasis, AIDS, malaria, influenza, COVID-19, etc [7,8]. On the contrary, the *NOS2*-mediated excessive NO production is associated with poor survival in cancer patients by increasing tumor aggressiveness, e.g., triple-negative breast cancer, *KRAS*-induced lung cancer, and colon adenomas [9–11]. The IFN-γ-induced NOS2-mediated hyperproduction of NO also imparts detrimental effects in several inflammatory and autoimmune diseases: Inflammatory bowel disease (IBD), Multiple Sclerosis, Rheumatoid arthritis, Systemic lupus erythematosus, encephalomyelitis, Sjogren's syndrome, sepsis, etc [12–18].

Chronic inflammatory diseases require maintenance treatment with non-steroidal anti-inflammatory drugs and managing disease exacerbation with steroidal medications. The long-term use of corticosteroid medications often leads to unavoidable adverse effects: steroidal resistance, osteoporosis, myopathy, osteonecrosis, adrenal insufficiency, opportunistic infections, etc. In ulcerative colitis, corticosteroids are used as mainstay treatment to manage flare-ups, yet almost 50% of the patients exhibit steroid resistance [19]. In addition, the therapeutic benefits of non-steroidal NOS inhibitors to treat inflammatory diseases have been questionable because of their mixed efficacies, adverse side effects, and unintended drug interactions [18,20]. These problems necessitate identifying alternative non-steroidal anti-inflammatory drugs, potently targeted to specific inflammatory axes, such as IFN-γ-induced NOS2-mediated hyperproduction of NO. In this study, our approach was to perform high-throughput screening of the Library of Pharmacologically Active Compounds (LOPAC®^{1280}) in an *in vitro* model of mouse tumor cell line H6 as these cells produce high amounts of IFN-γ-induced NO [2,21]. We also aimed to triage the hits from the screening, identify leads through validation and test their effects in orthogonal assays. Finally, we extended the assessment of the leads to primary mouse PMs and, more importantly, in the *in vivo* mice inflammatory disease models: dextran sodium sulfate (DSS)-induced ulcerative colitis and *Salmonella* Typhimurium-induced sepsis.

2. Materials and methods

2.1. Instruments and reagents

The list of instruments and reagents along with country of origin and catalog numbers are listed in supplementary Table 6.

2.2. Cell culture

H6 (hepatoma), Renca (renal adenocarcinoma), RAW 264.7 (monocyte/macrophage) cell lines, and primary mice PMs were maintained in Dulbecco's modified minimal essential medium-High Glucose (DMEM-HG), with 10% FBS. The media was supplemented with 5 μM β-mercaptoethanol, 100 μg/ml penicillin, 250 μg/ml streptomycin, 50 μg/ml gentamycin, and 2 mM glutamine (hereafter 10% DMEM). The cells were seeded in T75 flasks at 4-5 × 10^3 cells/mL density and maintained at 37 °C in a humidified incubator with 5% CO2 and 95% humidity. The spent cell culture media was replaced with fresh cell culture media after 36–48 h of growth in these flasks. The cells were passaged when 70–80% confluency was attained. Cell lines were passaged by treating with Trypsin-EDTA for 2–5 min at room temperature, and the reaction was stopped using an equal volume of 10% DMEM [2,21,22]. The cells were used for experimentation within passage 1–10. More detailed features of the cell lines used in this study are tabulated in supplementary Table 7.

2.3. Nitrite measurement

The production of nitric oxide (NO) was estimated by measuring the accumulated nitrite, the metabolic product of NO metabolism, in the medium using Griess reagent [23]. The reagent was prepared as a mixture of 1% (w/v) Sulfanilamide and 0.1% (w/v) N-(1-Naphthyl) ethylenediamine dihydrochloride dissolved in 2.5% *ortho*-phosphoric acid. The reaction mixture for the assay consisted of 25 μL of the cell-free supernatant, 25 μL of 10% DMEM, and 100 μL of Griess reagent that were mixed well. The absorbance was measured at 550 nm using a microtiter plate reader (Molecular Devices, Downingtown, PA, USA). The amount of nitrite in the supernatants was calculated from a standard curve of sodium nitrite (1.22 – 625 μM).

2.4. Compound library

The Library of Pharmacologically Active Compounds (hereafter named LOPAC®^{1280}) is a library of 1,280 off-patent small molecules. This biologically annotated collection of compounds is a set of pharmaceutically relevant structures that impact most signaling pathways and covers all major drug target classes. Several compounds are approved (FDA, EMA, and other drug regulatory bodies) and marketed drugs. The compounds are arranged in 96-well format in 16 racks of 80 and provided at a concentration of 10 mM in absolute DMSO.

2.5. LOPAC®^{1280} screening on H6 cells

On the day before the experiment, H6 mouse hepatoma cells were seeded at a density of ~ 1 × 10^4 cells/well of 96-well plates in 10% DMEM. The cells were maintained at 37 °C in a humidified incubator (Sanyo, UK) with 5% CO_2 for 8–12 h. The compounds were then diluted to treat the H6 cells. DMSO was toxic for H6 cells above 1% of the final solvent concentration. Therefore, the DMSO-induced-cytotoxic effect was eliminated by diluting all compounds in 10% DMEM to reduce DMSO solvent final concentration to 0.1%. The compounds were assayed in biological duplicates at 10 μM. The H6 cells were pre-incubated with the compounds for 15 min, followed by IFN-γ treatment and incubation for 24 h to identify the ones that reduced NO production. IFN-γ was added into all wells at a final concentration of 10 U/mL except in those labeled: 'Control,' 'LNMA,' and 'DMSO control.'

LNMA was used at 250 μM. 0.5% DMSO was added in 'DMSO control.' The H6 cells were incubated at 37 °C in a humidified incubator with 5% CO_2 for 24 h. The cell-free supernatant was collected for Griess assay for nitrite estimation.

2.6. Trypan blue dye exclusion assay

Trypan blue dye exclusion assay was performed to assay for percentage change in cell number [2]. Briefly, logarithmically growing cells were seeded at an initial density of 1×10^4 cells per well in a 96-well plate (0.15×10^6 cells per well for peritoneal exudate cells). The cells were treated with IFN-γ and compounds as indicated for 24 h. Adherent cells were harvested by adding 0.5% Trypsin-EDTA (HiMedia, India) per well. The cell suspension was mixed with an equal volume of 0.4% Trypan blue, and the number of live cells was counted in a hemocytometer.

2.7. Data analysis and selection of hits

The mean difference in nitrite concentrations upon compound treatment compared to IFN-γ was z-score transformed on GraphPad Prism software version 8.0.2. The dataset was transformed into a p-value using the normal cumulative distribution function of the z-score in the Microsoft Excel version 2211 and ranked based on the p-value. The q-values were derived from the rank and p-value using the 'MIN' function. The compounds with q-value < 0.5 (or z-score < -1.9) were assigned as hits and considered putative leads. The toxic hits identified in the counter screening for cytotoxicity were eliminated.

2.8. IC_{50} determination

The compounds were tested in 2-fold serial dilutions to inhibit nitrite production using Griess assay. The concentration ranges of the compounds tested are as follows: pentamidine isethionate (7.8–1250 nM), azithromycin dihydrate (1.25–40 μM), rolipram (0.0078–40 μM), auranofin (7.8–1000 nM), BIO, sanguinarine chloride, LP44, thapsigargin (7.8–500 nM), and ruthenium red (1.25–80 μM). Such concentration ranges were chosen to avoid toxic upper limits exceeding the CC_{90}. The dataset was transformed into the log scale for logarithmic interpolation. The maximal inhibitory response of the compounds was normalized to 0%. The non-linear regression fit was applied to calculate the IC_{50} value ranges and goodness of fit R^2 value.

2.9. RNA isolation and quantitative real-time PCR

RNA isolation from H6 cells was performed as previously described [21]. H6 cells were seeded in 6 well plates at a density of 3×10^5 cells per well. The cells were treated with IFN-γ (10 U/mL), pentamidine (1 μM), azithromycin (40 μM), rolipram (10 μM), and auranofin (1 μM) for 12 h. The cell lysates were prepared using TRI reagent. Phenol-chloroform extraction of RNA was performed. The mRNA from 1 to 3 μg total RNA was reverse transcribed to cDNA using a first-strand cDNA synthesis kit. qRT-PCR was performed with the following program: initial denaturation (95 °C for 10 min), denaturation (95 °C for 10 s), annealing (57 °C for 30 s), and extension (70 °C for 20 s). The denaturation to extension steps was repeated for 39 cycles. The Ct values of gene expression data were transformed to $2^{-\Delta\Delta Ct}$ and represented in the figures. The primer sequences are listed in supplementary Table 4.

2.10. Flow cytometry

The surface staining of MHC class 1 and intracellular ROS estimation was performed as previously described [2]. Briefly, H6 cells were cultured in 6 well plates at a density of 2×10^5 cells per well and treated with IFN-γ and lead compounds: pentamidine (1 μM), azithromycin (40 μM), rolipram (10 μM), and auranofin (1 μM) for 24 h. Cell surface staining for MHC class 1 was performed by incubating the cells in the blocking buffer for 30 min. The blocking buffer was prepared as 5% FBS and 0.1% (w/v) sodium azide in PBS. The cells were stained with the PE-conjugated anti-MHC Class 1 antibody at the dilution of 1:300. The cells were fixed with 4% paraformaldehyde. To estimate intracellular ROS, cells were incubated with 10 μM DCFDA dye at 37 °C water bath for 30 mins in the dark. Cell pellets were resuspended in 200 μL of PBS in all three cases. Data acquisition was performed in the BD FACSVerse™ flow cytometer and analyzed using BD FlowJo™ (BD Biosciences US).

2.11. PM harvesting from mice

C57BL/6 mice were bred and housed at a specific pathogen-free facility at the Central Animal Facility at the Indian Institute of Science (Bangalore, India). Six-to-eight-week-old male mice with body weights ranging from 20 to 25 g were used for all experiments. Peritoneal exudate cells were harvested directly from peritoneal cavity to obtain resident PMs, as previously described [22,24]. To harvest TG-elicited PMs, 4% Brewer's thioglycolate broth was prepared, autoclaved, and aged for at least 1 month before use. Mice were euthanized 96 h after i.p. injection of 1 ml of 4% Brewer's thioglycolate. Peritoneal cells were harvested and seeded in a 96-well plate at a density of $0.15x10^6$ cells per well. To isolate non-adherent peritoneal cells, the non-adherent cells were washed away after 1 h of seeding [22]. The Institutional Animal Ethics Committee approved all procedures (IAEC) constituted per article number 13 of the CPCSEA rules laid down by the Government of India (CAF/ethics/805/2021).

2.12. ELISA

IL6 and TNFα amounts in cell-free culture supernatants or sera were estimated using eBioscience™ ELISA Ready-SET-Go™ kit, per manufacturer's instructions [25].

2.13. In vivo DSS-induced ulcerative colitis and Salmonella Typhimurium-induced sepsis

DSS-induced ulcerative colitis was induced in mice, as previously described [25]. Colitis was induced by administrating 2% (w/v) DSS in drinking water for seven consecutive days (starting from day 0), as described in Fig. 7A. The mice were monitored for changes in body weight, stool consistency, and hematochezia. The disease activity index (DAI) was scored as described previously [26]. A 20% reduction in the body weight change was considered the humane endpoint. To test the role of immune nitric oxide, *Nos2*$^{-/-}$ mice were compared with C57BL/6 mice by dividing them into groups (n = 3–6 each): untreated control and colitic for WT and *Nos2*$^{-/-}$. To test the effect of leads *in vivo*, mice were randomly divided into several groups (n = 3–7 each): vehicle control, colitis, and the colitis groups receiving the lead compounds. The lead compounds were intraperitoneally injected at 10 mg/kg on day 2 and day 4. On day 7, animals were sacrificed, and the endpoint analyses were performed.

In the case of sepsis, BALB/c mice were injected intraperitoneally with $2–5 \times 10^6$ CFU of *Salmonella* Typhimurium bacterial culture grown for 3–5 hr. Each condition consisted of 6 male mice aged 6–8 weeks with a body weight of 22–24 g. The detailed protocol was previously described [17,27], and the compounds were injected intraperitoneally 3–4 h post-infection with pentamidine (1 and 10 mg/kg) or auranofin (0.3 and 1 mg/kg). The survival of the mice was monitored until 72 h post-infection.

The essential information concerning ARRIVE guidelines is tabulated for reference (supplementary Table 8). The Institutional Animal Ethics Committee approved all procedures (IAEC) constituted per article number 13 of the CPCSEA rules laid down by the Government of India (CAF/ethics/805/2021).

2.14. Statistical analyses

All graphical representations and statistical analyses were performed on GraphPad Prism software version 8.0.2. All data are represented as mean ± standard deviation of the mean (SD) unless stated otherwise. The data distribution was tested using QQ-plot to examine the skewness. Statistical analyses were performed using ordinary One-way ANOVA with Sidak's multiple comparisons tests and two-way ANOVA with Tukey's multiple comparisons tests. (ns), (*), (**), (***), (****) indicate non-significant difference and the statistical differences of $p < 0.05$, $p < 0.01$, $p < 0.001$, and $p < 0.0001$, respectively, between the comparable indicated, unless stated otherwise.

3. Results

3.1. Primary screen for inhibition of IFN-γ-induced NO production

Our previous studies demonstrated that IFN-γ leads to NO formation in several mice cell lines *in vitro*. The IFN-γ also activates transcriptional programs that can be categorized as NO-dependent and NO-independent pathways and the former lead to the blockade of cell cycle progression and induction of apoptosis [2,21]. The *in vitro* model of IFN-γ-activation of H6 cells was utilized to perform the primary screening to identify novel pharmacological modulators of IFN-γ-induced nitrite production using the Griess assay (Fig. 1A). First, we standardized the optimal conditions to conduct the large-scale screening, including the seeding density of H6 cells, concentration of IFN-γ, and the time-point for the end-point assay. The seeding density of H6 hepatoma cells was selected to be 1×10^4 cells in each well because it attained 60–70% confluency after 8 h of seeding. H6 cells produced nitrite in the concentration-dependent manner of IFN-γ. IFN-γ at 10 U/mL produced saturating amounts of nitrite after 24 h of incubation. The IFN-γ activation also reduced the percent change in cell number in a concentration-dependent manner (Fig. 1B, C; Fig. S1A). The assay signal dynamic range and data variation at the specified conditions were measured as screening window coefficient or Z′-factor [28]. The Z′-factor was calculated to be 0.49, indicating that the separation band is small but suitable for identifying leads.

For the primary screen, H6 cells were pre-treated with compounds from the LOPAC®^{1280} (Sigma) for 15 min, followed by IFN-γ treatment and incubation for 24 h to identify compounds that reduced NO production. The assay design is depicted in Fig. S1B and the plate-wise performance report of the positive controls from the primary screening is illustrated as a heatmap (Fig. S1C). The plate setup and full modulation profile of IFN-γ-induced NO production is represented (Fig. 1D, E). Lowered nitrite could be due to cell death caused by the

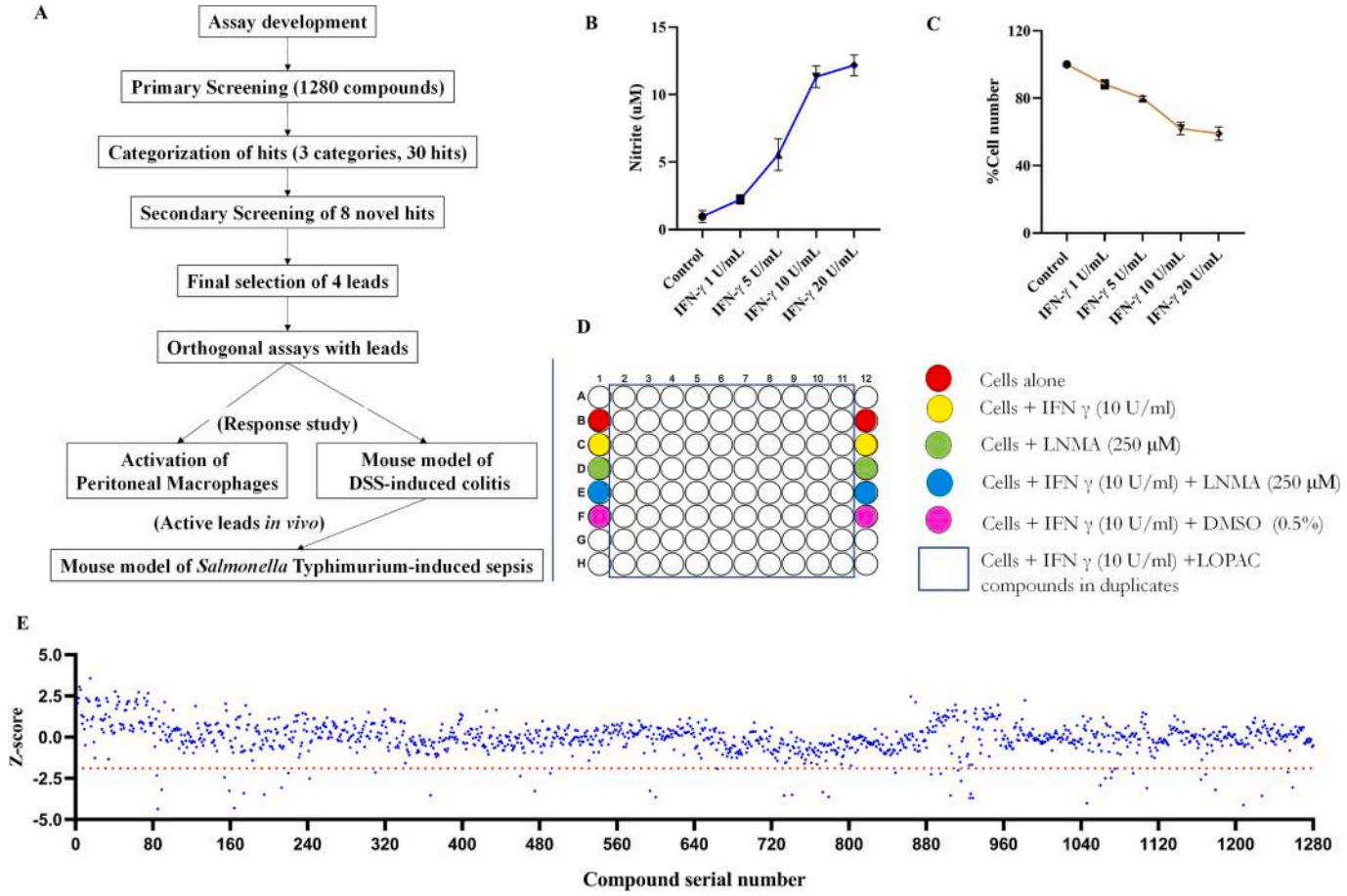

Fig. 1. Primary Screening of LOPAC®^{1280} in H6 hepatoma cell line for pharmacological inhibitors of IFN-γ-induced NO production. Large-library screening and downstream assays pipeline for the identification of pharmacological inhibitors of IFN-γ-induced NO production and anti-inflammatory effects (A). Concentration-dependent response of H6 hepatoma cells to IFN-γ with respect to nitrite production (B) and percent cell number change (C) after 24 h. The data representative of 3–4 independent experiments (B-C). The map of the 96-well plate used in the process of primary screening (D). Screening of 1280 pharmacologically active compounds from LOPAC®1280 was performed in the 96-well plate. The H6 hepatoma cells were seeded at a density of 1×10^4 cells/well and allowed to adhere for 6–8 h. The cell culture media was replaced with a fresh one to remove the floating cells. The cells were pre-treated with compounds for 15 min and treated with 10 U/mL of IFN-g for 24 h. The dot plot represents the data distribution. The dotted line in red represents the threshold for positive lead compounds. Numbers on the x-axis represent the serial numbers of the location of the compounds across 16 plates (E). Each data point is representative of mean + SD from 3 independent experiments. Each independent experiment involved a pair of biological replicates in 96-well plates. The measurements were recorded in technical duplicates (B, C).

toxicity of some compounds. Our counter screening for cytotoxicity identified 22 compounds that imparted cytotoxic effects (supplementary Table 1).

The mean difference of nitrite concentration between IFN-γ alone positive control and all the duplicate test compounds were z-score transformed. The z-scores were used to calculate the p-value and q-values. The compounds with q-value < 0.5 (or z-score < -1.9) were assigned as putative leads. A negative Z-score indicates the inhibition of nitrite formation.

3.2. Categorization and secondary screen for the validation of hits

The selected hits were categorized into known NOS inhibitors, steroidal compounds, and novel hits. The compounds in each category are listed in Table 1. Steroidal compounds are well-known for their global anti-inflammatory effects and are known to suppress IFN-γ signaling [29,30]. The presence of known NOS inhibitors and steroidal compounds indicated that the primary screening successfully identified the inhibitors of NO production.

We proceeded with the novel hits to identify compounds that were truly active against IFN-γ-induced nitrite formation and eliminate the false positives. The top six novel hits were auranofin, pentamidine, LP44, BIO, azithromycin and sanguinarine chloride. A few more compounds among the top twenty were tested in a concentration–response assay in the H6 hepatoma cell line. Cyclosporine, ruthenium red, LP44, and thapsigargin failed to fit the regression analysis, implying that these were false positives (data not shown). All other selected hits were fit in the curve, and the nonlinear regression curves were generated (Fig. 2). Finally, the lead compounds were chosen based on the R^2 values > 0.7. The goodness of fit in descending order were: auranofin, azithromycin, rolipram, and pentamidine (Fig. 2). The level of nitrite formation was reduced maximally in auranofin treatment, followed by rolipram, azithromycin, pentamidine (Fig. 3A).

Dexamethasone was assayed in parallel because this glucocorticoid can represent the steroidal compounds in the list of hits and is a robust positive control to inhibit IFN-γ signaling [30]. Dexamethasone showed the best fit in reducing the IFN-γ-induced NO production with the lowest IC_{50} value range of 6.7–8.1 nM and the best R^2 value of 0.97. This indicated that the concentration-dependent assay for secondary screen was suitable for the selection of the leads (Fig.S2).

IFN-γ activation also leads to a reduction in percent change in cell number due to its blocking effects on the cell cycle and induction of apoptosis. It could be argued that the inhibitory effects of the hits could be due to further reduction in cell number. This was tested in the presence of the lead compounds upon IFN-γ treatment in a concentration-dependent manner using Trypan blue dye exclusion. Azithromycin did not affect the cell number reduction. Other lead compounds: pentamidine, rolipram and auranofin significantly rescued the IFN-γ-induced reduction in cell number (Fig. 3B).

To rule out that the effects of top four leads was not specific to H6 cell line-specific, these were tested in RAW 264.7 (monocyte/macrophage) and Renca (renal adenocarcinoma) mouse cell lines. These cell lines were selected because they phenocopy H6 cells by producing NO upon IFN-γ activation. All the leads except azithromycin significantly reduced the formation of IFN-γ-induced NO in the RAW 264.7 cell line. Similarly, all the leads except rolipram reduced the formation of IFN-γ-induced NO

Table 1
Categorization of the top hits.

Plate S.No. (LOPAC®^{1280})	Name	Class	Selectivity	Z-score	p-value	q value
Category 1: NOS inhibitors						
85	(±)-AMT hydrochloride	Nitric Oxide	iNOS	−4.36	6.44E-06	0.004985
491	S-Ethylisothiourea hydrobromide	Nitric Oxide	NOS	−2.20	0.013647	0.45249
848	NG-Nitro-L-arginine methyl ester hydrochloride	Nitric Oxide	NOS	−2.17	0.014886	0.464734
Category 2: Steroidal compounds						
174	Budesonide	Hormone	Cortisol	−3.40	0.000325	0.026014
159	Beclomethasone	Hormone	Glucocorticoid	−3.27	0.000525	0.033633
594	Hydrocortisone	Hormone	Cortisol	−3.27	0.000526	0.033633
1179	Triamcinolone	Hormone	Glucocorticoid	−3.20	0.000669	0.04032
213	Betamethasone	Hormone	Glucocorticoid	−3.07	0.001051	0.056027
895	Progesterone	Hormone	Progesterone	−2.22	0.013029	0.450729
220	Corticosterone	Hormone	Glucocorticoid	−2.18	0.014365	0.459682
Category 3: Novel hits						
1046	Auranofin	Phosphorylation	(Not listed)	−4.02	2.89E-05	0.009245
925	Pentamidine isethionate	Glutamate	NMDA	−3.69	0.000109	0.021544
926	LP44	Serotonin	5-HT7	−3.45	0.000278	0.023763
773	BIO	Phosphorylation	GSK-3alpha/beta	−3.35	0.000402	0.030266
89	Azithromycin dihydrate	Immune Cell Signaling	50S subunit	−3.19	0.000693	0.04032
1108	Sanguinarine chloride	Ion Pump	Na+/K + ATPase	−3.10	0.000945	0.052585
916	Picrotoxin	GABA	GABA-C	−2.66	0.003865	0.18323
1164	Tetraethylthiuram disulfide	Biochemistry	Alcohol Dehydrogenase	−2.57	0.004955	0.226517
242	Cyclosporin A	Phosphorylation	Calcineurin phosphatase	−2.51	0.005981	0.263186
1065	SB-366791	Vanilloid	VR1	−2.50	0.006168	0.263186
1071	Ruthenium red	Ion Pump	Mitochondrial uniporter	−2.47	0.006606	0.272782
84	Adenosine 3′,5′-cyclic monophosphate	Phosphorylation	PKA	−2.33	0.009742	0.366747
885	(±)-Octoclothepin maleate	Dopamine	D2	−2.26	0.011707	0.418331
1169	BAY 61–3606 hydrochloride hydrate	Phosphorylation	Tyrosine kinase	−2.26	0.011766	0.418331
1094	Sobuzoxane	Gene Regulation	Topo II	−2.20	0.013787	0.45249
1254	Tyrphostin A9	Phosphorylation	PDGFR	−2.12	0.016668	0.496155
1072	Rolipram	Cyclic Nucleotides	PDE IV	−2.09	0.018176	0.528754
913	Sodium Oxamate	Biochemistry	Lactate Dehydrogenase	−2.02	0.021671	0.616418
664	p-Iodoclonidine hydrochloride	Adrenoceptor	alpha2	−1.93	0.026573	0.73477
1075	7,8-Dihydroxyflavone hydrate	Cytokines, Growth Factors and Hormones	TrkB	−1.92	0.02698	0.73477

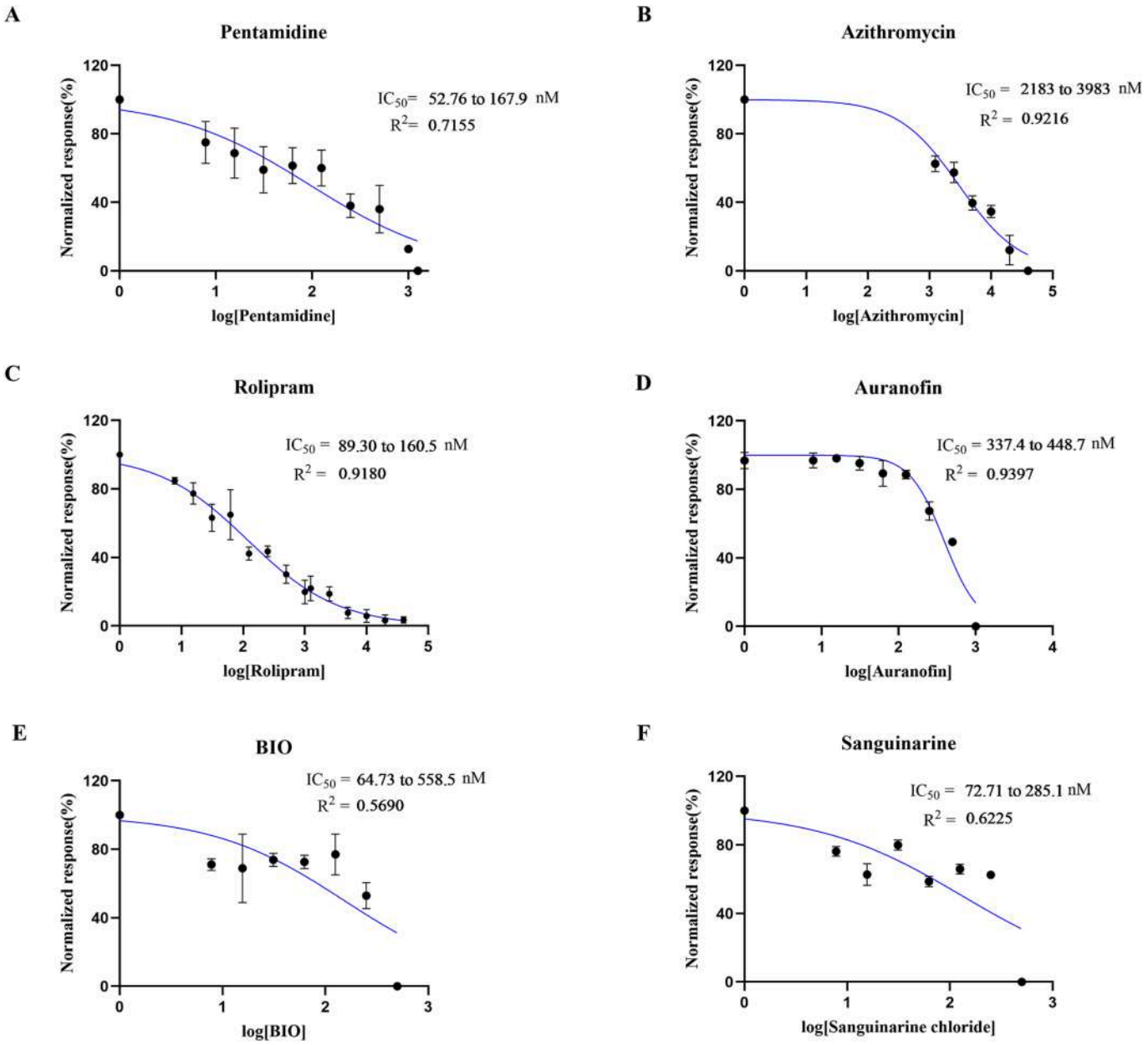

Fig. 2. Dose response curves of selected lead compounds. The concentrations of compounds are presented in log scale and dose response curves were generated using GraphPad Prism software. The IC_{50} value (50% inhibition) range was calculated on the profile likelihood of 95% confidence interval. R^2 value is represented as the goodness of fit. Each datapoint is representative of mean ± SD from 3 independent experiments. Each independent experiment involved a pair of biological replicates in 96-well plates. The measurements were recorded in technical duplicates.

in the Renca cell line (Fig. S3). In addition, pentamidine rescued the IFN-γ-induced reduction in percent change in cell number in both RAW 264.7 and Renca cell lines. Azithromycin showed similar effect in Renca cell line (Fig. S4). Overall, this indicates that the effects observed were not cell-specific.

3.3. Orthogonal assays to deduce plausible mechanism

The biological response of IFN-γ requires a complex network of multiple signaling pathways. IFN-γ canonically activates the JAK-STAT pathway to induce the expression of transcription factors. These hierarchically activate a cascade of primary response by STAT1, then the secondary response by IRF1, and so on. The NO-independent transcriptional program includes the induction of inflammatory genes, notably *Irf1* (Interferon regulatory factor 1), *Socs1* (suppressor of signal), *Tap2* (antigen processing), and *Cd274* (encodes PD-L1, suppressing immune response). Seminal research on the mechanism of IFN-γ-induced *Nos2* transcription in macrophage cell lines demonstrated that the phosphorylation cascade in the JAK-STAT pathway involving JAK2, MEK1/2, Erk1/Erk2, and STAT1α are vital players in the process [31]. The transcription factors like IRF1 and NF-kB, activated in the primary response of IFN-γ, are also crucial binding factors upon the *Nos2* promoter to initiate transcription. The *Nos2* transcription is driven by several transcription factors synergistically [8,31,32]. Although the precise mechanism in the H6 hepatoma cell line is unknown, the primary processes behind IFN-γ-induced *Nos2* transcription are expected to be broadly similar. The transcriptional program of *Nos2* (Nitric Oxide Synthase 2 in NO production) upon IFN-γ-activation in H6 cells is NO-dependent [21]. The effects of the top four compounds from orthogonal assays in transcriptional activation of IFN-γ-activated H6 cells was

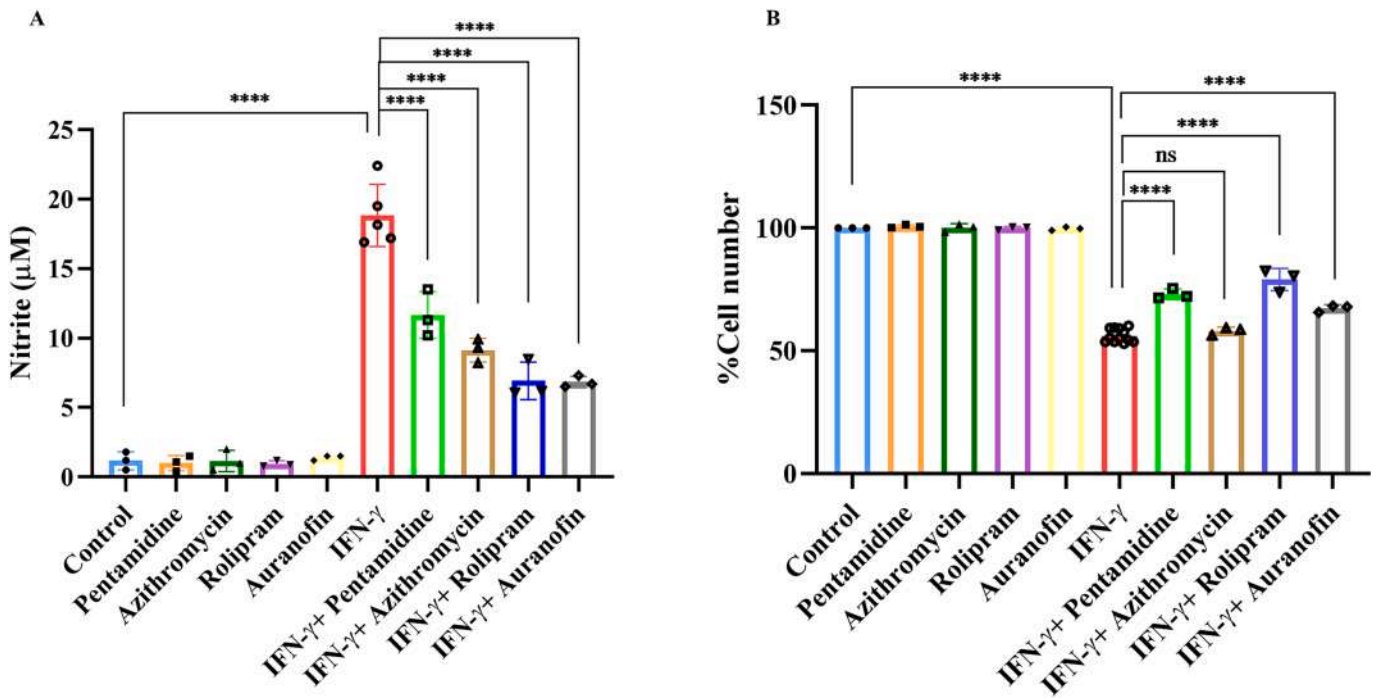

Fig. 3. The lead compounds significantly reduce nitrite production. H6 hepatoma cells were seeded at the density of 1×10^4 cells in each well of 96-well plate. Following ~ 8 h of incubation, the cell culture supernatant was removed to get rid of dead or non-adherent cells. The cells were co-treated with IFN-γ and the lead compounds: Pentamidine (1 μM), Azithromycin (40 μM), Rolipram (10 μM) and Auranofin (1 μM). The concentration of nitrite in cell-free supernatant was estimated (A). The percent cell number was measured using Trypan blue dye exclusion assay (B). The statistical analyses were performed using ordinary One-way ANOVA with Sidak's multiple comparisons test. (ns), (*), (**), (***), (****) indicate non-significant difference and the statistical differences of $p < 0.05$, $p < 0.01$, $p < 0.001$, and $p < 0.0001$ between the comparable indicated. Each datapoint is representative of mean ± SD from independent experiments. Each independent experiment involved a pair of biological replicates in 96-well plates. The measurements were recorded in technical duplicates.

evaluated for the genes mentioned earlier. Furthermore, the influence of the compounds on the surface expression of MHC Class 1 and intracellular ROS production in IFN-γ-activated H6 cells was studied using flow cytometry.

To test the transcriptional response, H6 cells were incubated with the leads in the presence of IFN-γ for 12 h. Expectedly, a significant induction of *Irf1*, *Tap2*, and *Cd274* genes was observed upon IFN-γ activation compared to untreated control. The expression of *Socs1* remained unaffected. None of the lead compounds significantly affected IFN-γ-induced *Irf1* or transcription. The IFN-γ-inducible transcription of *Tap2* and *Cd274* was significantly upregulated in the presence of rolipram but unaffected by other compounds. Except for pentamidine, all the lead compounds significantly downregulated the IFN-γ-induced transcription of *Nos2* (Fig. 4).

To understand whether the altered transcription profile affected the surface expression of MHC Class I and intracellular ROS, the compounds-treated IFN-γ-activated H6 cells were subjected to flow cytometric analysis. None of the compounds was found to affect the IFN-γ-induced surface expression of MHC Class I. However, all compounds significantly reduced the IFN-γ-induced enhanced level of intracellular ROS (Fig. 5).

The excessive production of IFN-γ-induced NO leads to the blockade of cell cycle progression [21]. This is presumably due to erroneous DNA replication in the presence of NO-mediated oxidative stress. Therefore, a flow-based cell cycle analysis was performed to obtain a detailed insight into the functional effects of the compounds on H6 cell cycle arrest mediated by IFN-γ signaling. The propidium iodide staining provided a quantitatively comparable measurement of the intracellular DNA content. IFN-γ activation led to a significant increase in the S phase population, indicating an arrest of the cell cycle at the G_2-M checkpoint. Consequently, IFN-γ-activation significantly reduced the G_2-M population. None of the compounds significantly increased the sub-G_1 phase population, indicating no remarkable toxicity leading to DNA damage. Pentamidine showed no distinguishable effect on IFN-γ-induced cell cycle alterations. Rolipram significantly increased IFN-γ-mediated reduction in G_2-M cells. Azithromycin, rolipram and auranofin significantly rescued the IFN-γ-induced arrest of cells at the S phase (Fig.S5).

3.4. Assessment of the effects of the lead compounds on activated mouse PMs

Primary mechanistic investigations in mouse cell lines showed that the leads are potent in suppressing IFN- γ -induced NO production. These observations led us to evaluate the leads in primary mouse macrophages *ex vivo*. Therefore, we sought to assess the effects of the leads on IFN-γ-activated PMs. Resident and Thioglycolate (TG)-elicited PMs were studied separately in the presence of the leads. TG-elicitation facilitates sterile inflammation in the peritoneal cavity, as it recruits small PMs at the site. These are physically, functionally, and developmentally distinct from the large resident PMs [24,33]. Studying both PM types helped to understand the effects of leads in different macrophage subsets. Among the leads tested, only auranofin significantly reduced the IFN-γ-induced nitrite production from both PM types (Fig. 6). The inhibitory response was concentration-dependent without cytotoxicity at a non-toxic concentration of 0.5 μM (Fig.S6). IFN-γ activation did not induce TNFα production in the TG-elicited PMs. However, pentamidine, azithromycin, and auranofin significantly reduced the IFN-γ-induced IL6 production from TG-elicited PMs (Fig. 6 E, F).

3.5. Evaluation of the four leads in an in vivo model of colitis in mice

The orthogonal assays in H6 cell lines and *ex vivo* tests on PMs indicated that these lead compounds may display anti-inflammatory effects. Dextran Sodium Sulfate (DSS) and 2,4,6-Trinitrobenzene

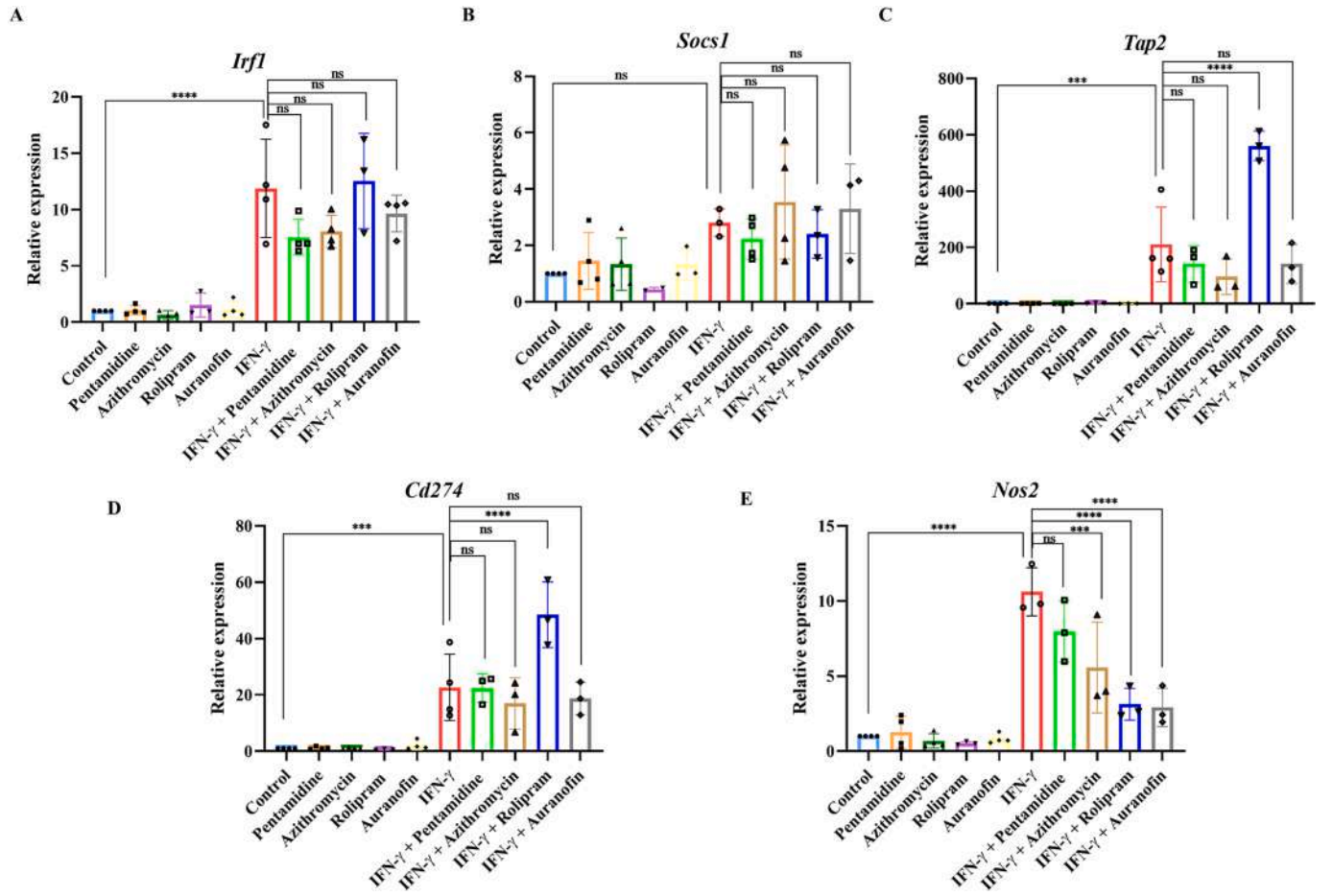

Fig. 4. RT-qPCR-based profiling of the modulation of IFN-γ-induced transcriptional program in response to lead compounds. H6 hepatoma cells were seeded at the density of $3x10^5$ cells in each well of 6-well plate. Following ~ 8 h of incubation, the cell culture supernatant was removed to get rid of dead or non-adherent cells. The cells were co-treated with IFN-γ and the lead compounds: Pentamidine (1 μM), Azithromycin (40 μM), Rolipram (10 μM) and Auranofin (1 μM). The RNA was isolated after 12 h of treatment and reverse transcribed for qPCR analysis of the genes *Irf1* (A), *Nos2* (B), *Tap2* (C), *Cybb* (D), *Cd274* (E), and *Socs1* (F). *Actb* was used as reference gene for determining the $2^{-\Delta Ct}$. The $2^{-\Delta\Delta Ct}$ was determined from untreated controls and denoted as relative expression. The statistical analyses were performed using ordinary One-way ANOVA with Sidak's multiple comparisons test. (ns), (*), (**), (***), (****) indicate non-significant difference and the statistical differences of $p < 0.05$, $p < 0.01$, $p < 0.001$, and $p < 0.0001$ between the comparable indicated. The data is representative of 3–4 independent experiments. Each independent experiment represents a biological replicate performed in a 6-well plate. The measurements of the Cq values were recorded in technical triplicates.

sulfonic acid (TNBS) -induced colitis are widely used as *in vivo* mouse ulcerative colitis models. TNBS-induced colitis primarily depends on the Th1 response and CD4 + T cells [34]. In contrast, DSS-induced colitis depends on CD4 + T cells, macrophages, and neutrophils, where IFN-γ signaling plays a vital role in disease pathogenesis [25,35,36]. Therefore, we tested the usefulness of the identified lead compounds in DSS-induced ulcerative colitis. Initially, we tested the role of NOS2 in the disease pathogenesis of DSS-induced colitis. *Nos2*$^{-/-}$ mice were compared against the wild-type counterparts in the progression of colitis and the outcome. Assessments with respect to colon length and DAI presented significant beneficial effects in the absence of the *Nos2* gene (supplementary Table 2, Fig.S7). *Nos2*$^{-/-}$ mice proved to be significantly resistant in the development of colitis, indicating that the presence and expression of the NOS2 play pivotal detrimental roles in colitis pathogenesis. This observation also suggested that inhibitors of IFN-γ-signaling-induced NOS2 activity could be advantageous as anti-inflammatory molecules against colitis.

Next, we tested the lead compounds in the mouse model of colitis. The compounds were injected intraperitoneally at 10 mg/kg body-weight on days 2 and 4 of the commencement of oral DSS treatment. The mice were compared to wild-type mice, intraperitoneally injected with an equal dosage of DMSO as vehicle control. The treatment of azithromycin failed to improve the percent change in body weight. Although it could slightly improve the colon length but was not significant due to variability. Rolipram showed a significant effect but displayed high variability. Pentamidine and auranofin proved to be significantly more beneficial than rolipram in rescuing the percent change in mouse body weight. A similar trend with statistical significance is reflected in the comparison of DAI (supplementary Table 3). Pentamidine and auranofin could significantly recover the DSS-induced reduction in colon length and improve DAI. On the other hand, the development of ulcerative colitis did not elevate serum TNFα, but significantly increased IL6. Pentamidine, rolipram and auranofin reduced serum IL6, however, the effect of pentamidine was statistically significant (Fig. 7). The overall *in vivo* assessment showed that pentamidine and auranofin have much better *in vivo* anti-inflammatory activities than others in colitis.

3.6. Pentamidine and auranofin improve survival of mice during sepsis

It was important to address whether these two compounds were effective in another inflammatory disease mice model. Therefore, we induced peritonitis sepsis by intraperitoneal injection of *Salmonella* Typhimurium in mice [17,27]. To mimic the clinical scenario, the compounds were intraperitoneally injected after 3–4 hr post injecting the bacteria. Pentamidine proved to be significantly effective at 10 mg/

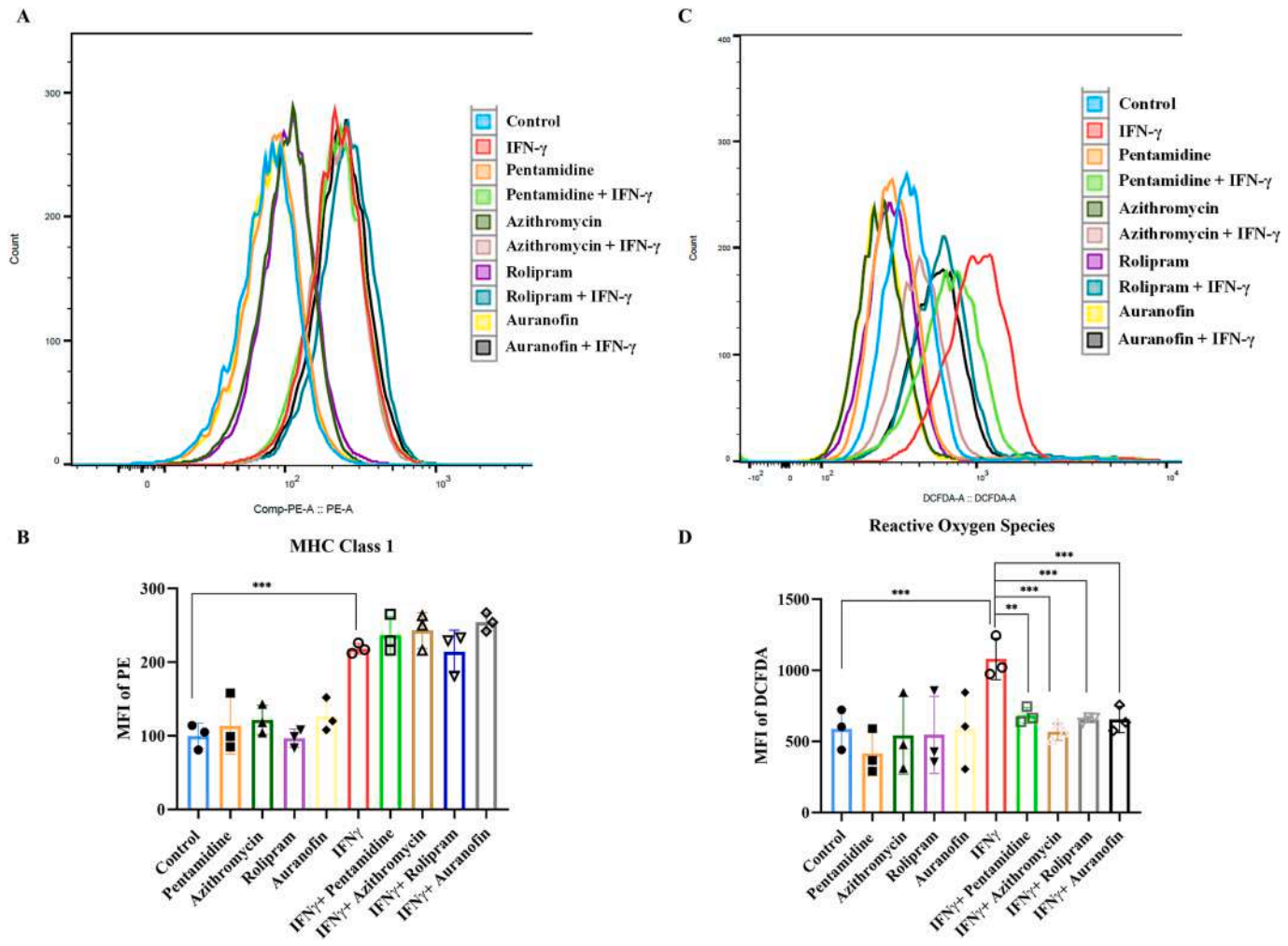

Fig. 5. The lead compounds lower IFN-γ-induced ROS formation without affecting surface expression of MHC class 1. The surface expression of MHC Class 1 (A, B) and intracellular level of ROS (C, D) were enumerated using flow cytometry in H6 cells. The lead compounds: pentamidine (1 μM), azithromycin (40 μM), rolipram (10 μM), and auranofin (1 μM) were cotreated with IFN-γ for 24 h prior to the analysis. The statistical analyses were performed using ordinary One-way ANOVA with Sidak's multiple comparisons test (B-H). (ns), (*), (**), (***), (****) indicate non-significant difference and the statistical differences of $p < 0.05$, $p < 0.01$, $p < 0.001$, and $p < 0.0001$ between the comparable indicated. Data is represented as mean ± SD of 3 independent experiments, each datapoint in the graph representing an independent experiment. Each independent experiment represents a biological replicate performed in a 6-well plate. (B, D).

kg body weight dose in improving the survival of mice in sepsis. Auranofin greatly enhanced survival at 0.3 and 1 mg/kg body weight doses. The Kaplan-Meier survival analysis demonstrated that the median survival of pentamidine at 10 mg/kg body weight and auranofin at 0.3 mg/kg body weight treatment improved to 60 and 66 h, respectively, in comparison to untreated septic mice, which were 24 h (Fig. 8). The log-rank test for trend showed a p-value of < 0.0001, indicating statistical significance for the survival of compound-treated mice.

4. Discussion

The high-throughput screening of the LOPAC®^{1280} targeting IFN-γ-induced NO production led to the identification of four novel pharmacological inhibitors of the inflammatory signaling process: pentamidine, azithromycin, rolipram, and auranofin. The primary targets of the lead compounds are as follows. Pentamidine is an NMDA receptor antagonist and used to treat *Pneumocystis* pneumonia, leishmaniasis, and trypanosomiasis [37]. Also, pentamidine is reported to bind tRNA non-specifically and dampen translational processes [38]. Azithromycin binds to the 50S subunit of the 70S bacterial ribosome to block translation [39]. It is used against bacterial infections as an antibiotic and cystic fibrosis due to its anti-inflammatory properties [40]. Rolipram inhibits phosphodiesterase 4 (PDE4) and elevates intracellular cyclic AMP (cAMP) [41]. Auranofin, a gold(I) compound with phosphine and thiol ligands in a linear arrangement, primarily inhibits thioredoxin reductase [42], which is critically involved in maintaining normal protein function and combating oxidative damage. Auranofin is typically used in combination with other medications, such as non-steroidal anti-inflammatory drugs (NSAIDs) or disease-modifying antirheumatic drugs (DMARDs), to help control the symptoms of rheumatoid arthritis [43]. However, the clinical use of auranofin against rheumatoid arthritis declined in the last decade. The decline may be due, in part, to the inclusion of more effective DMARDs, such as methotrexate [44]. Nevertheless, auranofin presents an excellent potential for drug repurposing in various diseases. Notably, auranofin inhibits SARS-CoV-2 replication, ACE-2-dependent SARS-CoV-2 endocytosis and also inhibits PLpro, the papain-like protease of SARS-CoV-2 [45,46]. In addition, auranofin's anti-inflammatory properties protect against neurodegenerative disorders, such as Alzheimer's and Parkinson's disease [47]. Three out of four leads, namely, auranofin (trade name: Ridaura), pentamidine (trade name: Pentam 300), and azithromycin (trade name: Zithromax), are FDA-approved marketed drugs. Rolipram is not FDA-approved because clinical trials of the drug have not consistently shown positive results. Alternatively, roflumilast (trade name: Daliresp) has the same activity as

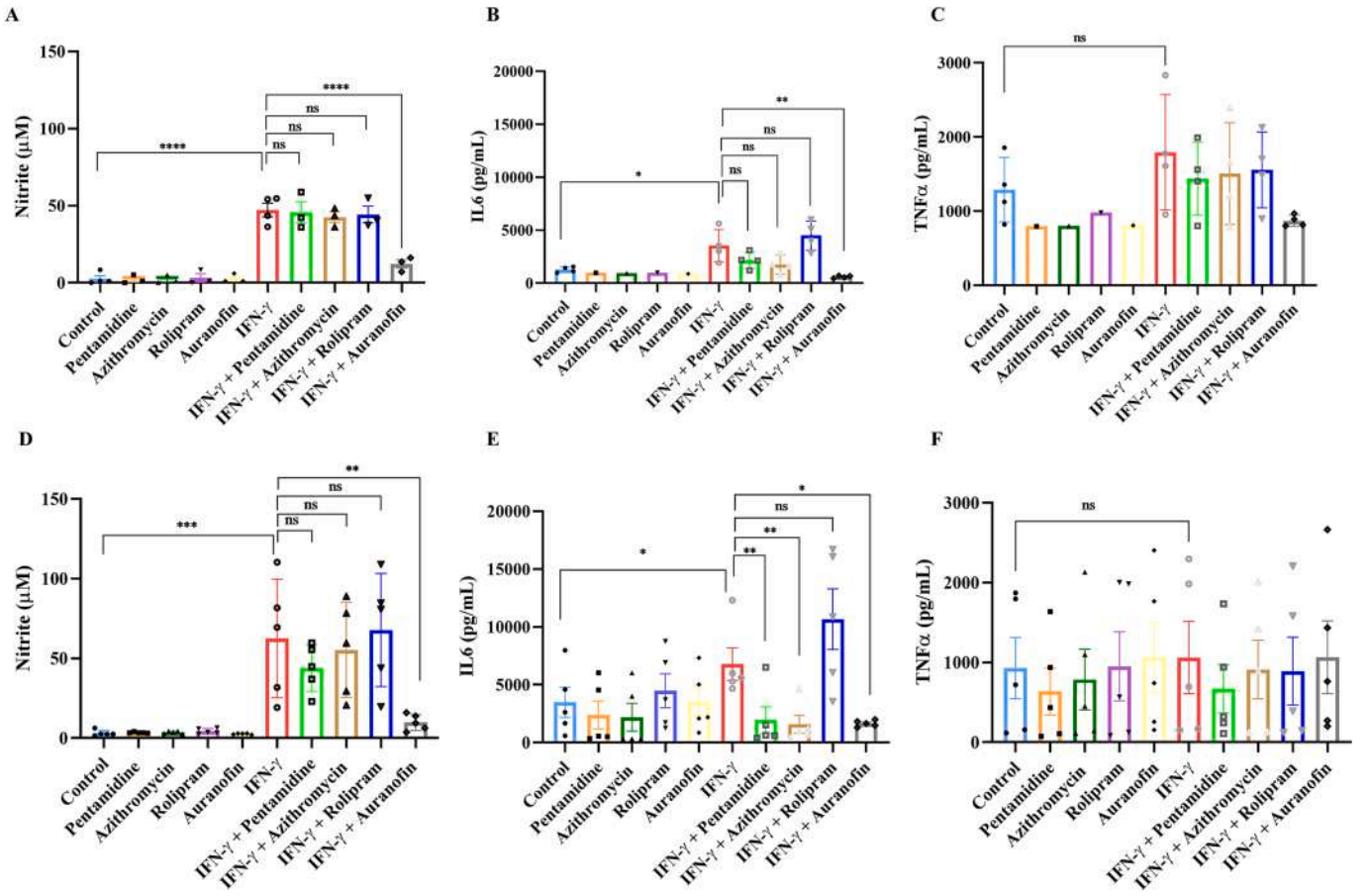

Fig. 6. Auranofin lowers IFN-γ-induced nitrite and IL6 production in resident and TG-elicited primary mouse PMs. Peritoneal macrophages were harvested from the peritoneal cavity of C57BL/6 mice and $2x10^5$ cells were plated in each well of a 96-well plate. The cells were co-treated with 10 U/mL of IFN-γ and the lead compounds at the indicated concentrations. The cell-free supernatant was assayed after 24 h for nitrite(A), IL6 (B) and TNFα (C). TG-elicited macrophages were harvested from the peritoneal cavity of C57BL/6 mice after 4 days of intraperitoneal TG-injection. $2x10^5$ cells were plated in each well of 96-well plate for the experimentation. The macrophages were co-treated with IFN-γ and the lead compounds. The cell-free supernatant was assayed after 24 h for nitrite(D), IL6 (E) and TNFα (F). The lead compounds were used at the following concentrations: pentamidine (1 μM), azithromycin (40 μM), rolipram (10 μM), and auranofin (0.5 μM). The statistical analyses were performed using ordinary One-way ANOVA with Sidak's multiple comparisons test (B-H). (ns), (*), (**), (***), (****) indicate non-significant difference and the statistical differences of $p < 0.05$, $p < 0.01$, $p < 0.001$, and $p < 0.0001$ between the comparable indicated. Each datapoint is representative of independent experiment. Data is represented as mean ± SD of 3 to 5 independent experiments, each datapoint in the graph representing data from one mouse.

rolipram and is a FDA-approved marketed drug.

A systematic evaluation of the leads in cell lines, primary mouse macrophages, and *in vivo* mouse disease model ranked auranofin as the top-active lead. This conclusion is comparatively drawn from the best goodness of fit on IFN-γ-induced NO production *in vitro*, the most effective transcriptional repression of IFN-γ-induced *Nos2* expression, the only compound to abolish NO production in activated primary macrophages, and the significant beneficial effect in DSS-induced mouse colitis. Based on *in vivo* experiments, pentamidine and auranofin emerged are the most potent compounds from the LOPAC®^{1280} library which can be repurposed for use in inflammatory diseases. A summary of the inhibitory effects of auranofin and pentamidine is depicted in Fig. 9. To understand the mechanisms by which these compounds may be affecting the IFN γ -induced NO pathway, further in silico studies were performed. SWISSTargetPrediction showed that pentamidine has a probability score of 1 for targeting proteases and family A G-protein coupled receptors. It may target 33.3% of family A G-protein coupled receptors (Fig. S8A). Molinspiration showed that pentamidine possesses a bioactivity score of 0.6 as a protease inhibitor and 0.35 as GPCR ligand (Fig. S8B). The IFN-γ-activated signaling pathway is less likely to be influenced by proteases unless the proteases proteolytically activate proteins assisting NOS2 function. It is more likely to be affected by the GPCR signaling pathway at the suboptimal concentration used in this study. Therefore, pentamidine's non-canonical modulation of the GPCR pathway may cause signaling crosstalk and underlie the reduction of nitrosative and oxidative effects of IFN-γ (Fig.S9). SWISSTargetPrediction also showed that auranofin may target 46.7% of kinases. Molinspiration showed that auranofin is predicted to have only enzyme inhibitor activity with a bioactivity score of 0.31 (Fig.S8 C, D). The IFN-γ signaling pathway largely depends on the phosphorylation cascade for transcriptional activation. For instance, the phosphorylation of transcription factors like IRF1 and NF-kB is essential for the IFN-γ-activated transcription of *Nos2*. Auranofin may inhibit some kinase functions to downregulate the *Nos2* transcription upon IFN-γ signaling (Fig.S9).

IFN-γ often imparts immunomodulatory and anti-tumor effects by regulating cell proliferation and survival. Several studies deciphered the mechanism of action in inflammatory conditions and malignancy [48,49]. For instance, in vitiligo, IFN-γ promotes the expression of pro-apoptotic factors Bax, Bak, and cleaved caspase-3 in melanocytes to induce apoptosis [50]. IFN-γ plays a crucial role in pushing Toll-like receptor-activated microglia towards neurotoxic states that lead to the emergence of energetic and oxidative stress, significant impairment in network functioning, and, ultimately, neuronal demise [51]. IFN-γ has

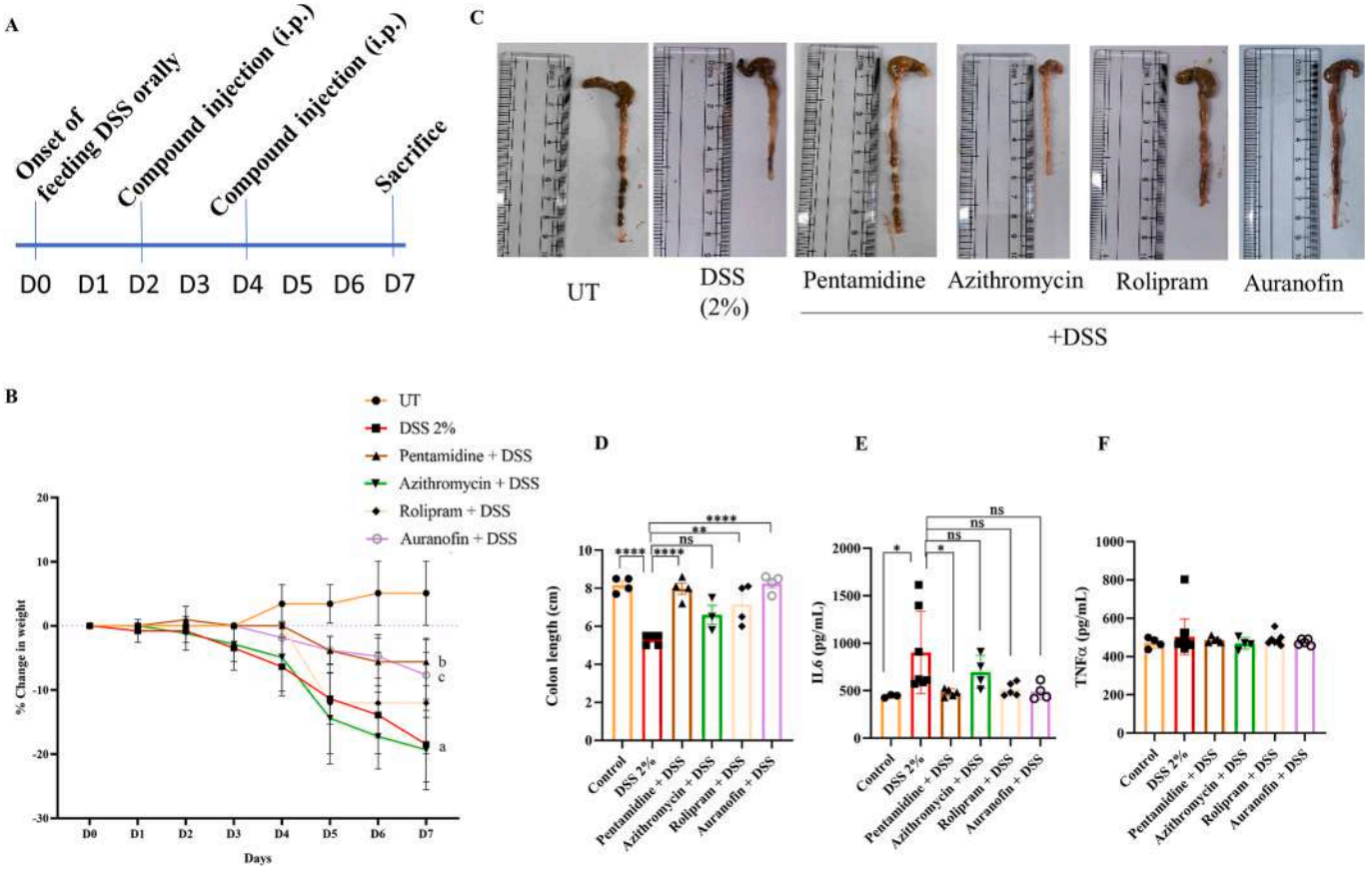

Fig. 7. Pentamidine and auranofin display the most potent anti-inflammatory effects in an *in vivo* model of DSS-induced mouse colitis. Wild-type C57BL/6 mice were challenged with DSS-induced colitis. The treatment timeline of DSS and lead compounds is depicted (A). Change in percent body weight across 7 days of DSS treatment (B). Photographs of the colon from cecum to rectum (C) and the bar diagram of the pooled data of colon length (D). The serum level of IL6 (E) and TNFα (F) after 7 days of DSS treatment. The statistical analyses were performed using two-way ANOVA with Tukey's multiple comparisons test (B) and ordinary One-way ANOVA with Sidak's multiple comparisons test (D, E, F). (a), (b) and (c) indicate (UT vs. DSS, $p < 0.001$), (DSS vs. Pentamidine + DSS, $p < 0.001$), and (DSS vs. Auranofin + DSS, $p < 0.001$) on day 7, respectively (B). (ns), (*), (**), (***), (****) indicate non-significant differences, and the statistical differences of $p < 0.05$, $p < 0.01$, $p < 0.001$, and $p < 0.0001$ between the comparable indicated (D, E, F). Each data point is representative of mean ± SD from 6 to 7 mice (B) or represents a mouse and cumulatively is depicted as mean ± SD (D, E, F).

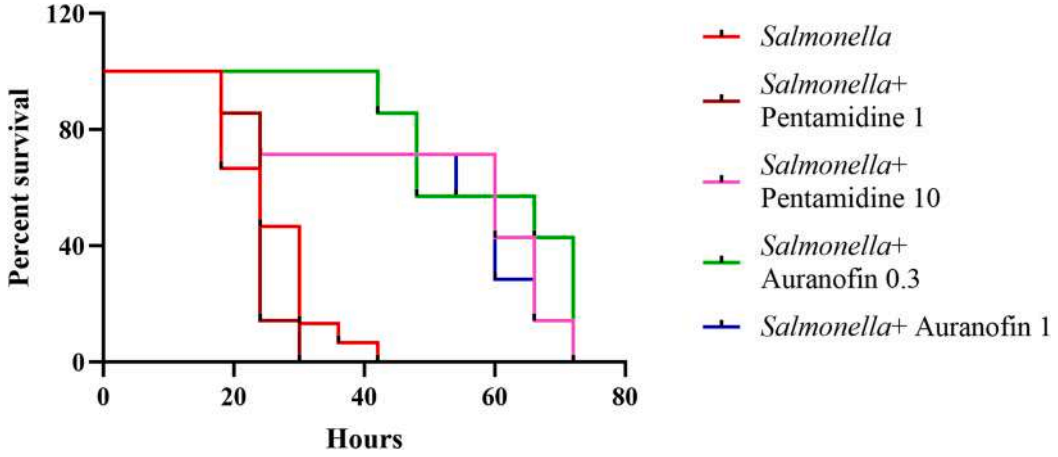

Fig. 8. Pentamidine and auranofin improve survival in peritonitis sepsis in mice. BALB/c mice were intraperitoneally injected with *Salmonella* Typhimurium to induce sepsis. Pentamidine and auranofin were intraperitoneally administered 3 h post infection. The numbers after compound names indicate the dosage in mg/kg body weight of mice. Each condition comprised of 6–9 mice of 6–8 weeks old and 22–24 g of body weight. The survival data is demonstrated as Kaplan-Meier plot.

dual effects in the tumor microenvironment, from tumor elimination to escape. Consequently, the interaction between IFN-γ and the immune system within the tumor determines the outcome of the tumor in a person with cancer [52]. Studies using several mouse tumor cell lines demonstrated that some tumor types are more selectively susceptible to IFN-γ-mediated cell cycle arrest and apoptosis. A mechanistic investigation on IFN-γ-mediated tumor apoptosis revealed that the cell proliferation blockade and apoptosis in H6 hepatoma and L929 fibrosarcoma

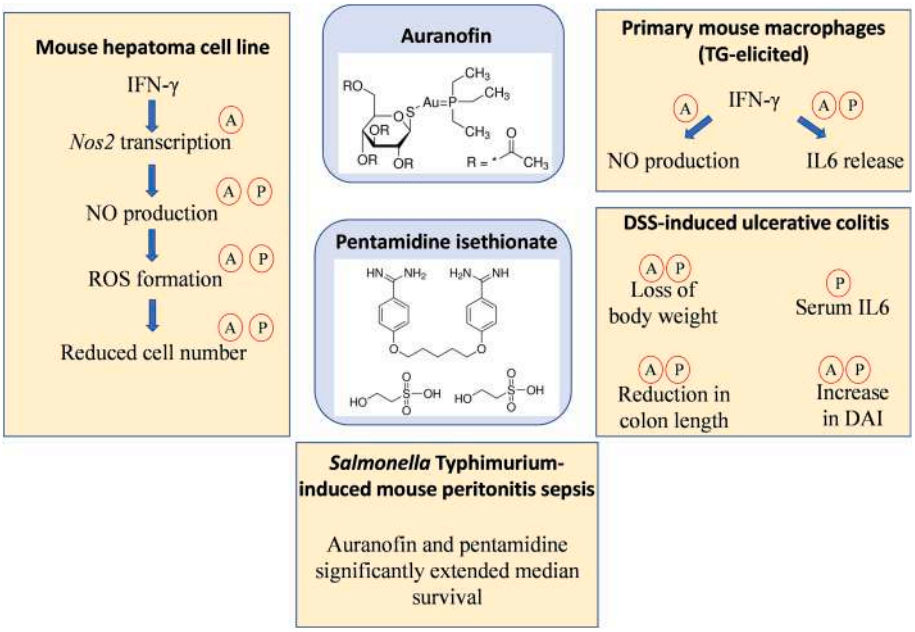

Fig. 9. A model depicting the role of auranofin and pentamidine as anti-inflammatory compounds in *in vitro* and *in vivo* settings. The figure depicts the summary of the inhibitory effects of the top two lead compounds: auranofin and pentamidine. The chemical structures of the lead compounds are depicted in the middle. In this figure, 'A' and 'P' indicate the inhibitory effect of auranofin and pentamidine respectively in the cellular and biological processes mentioned. The effects are categorized in mouse hepatoma cell line H6, TG-elicited primary mouse macrophages and DSS-induced mouse ulcerative colitis. Auranofin significantly reduced the IFN-γ-induced nitrite production by reducing transcription of *Nos2*, whereas pentamidine presumably affected at the post-transcriptional level to reduce nitrite. All these culminated into the reduction of intracellular ROS and increased cell survival in the presence of IFN-γ. Pentamidine reduced the IFN-γ-induced IL6 production from TG-elicited primary mouse macrophages, whereas auranofin potently reduced IFN-γ-activated nitrite and IL6 production. Importantly, auranofin and pentamidine demonstrated protective effects in DSS-induced mouse ulcerative colitis *in vivo*. Also, auranofin and pentamidine significantly extended the survival of mice during *Salmonella* Typhimurium-induced sepsis.

mouse cell lines depend on IFN-γ-induced NOS2-mediated NO production. NO elevates intracellular peroxynitrite and ROS and activates the Jnk pathway, culminating in cell death [2,21]. The IFN-γ-activation also reduces cell number in the Renca renal adenocarcinoma cell line [50,53]. This study demonstrates that all four leads effectively reduced IFN-γ-induced NO production in at least two of three cell lines H6, RAW 264.7, and Renca. Pentamidine inhibited IFN-γ-mediated NO production and rescued cell numbers in all three cell lines to different extents, indicating that its effects are not cell-line restricted. Although auranofin effectively retarded the NO production in these cell lines, it rescued IFN-γ-mediated cell number reduction only in H6. The underlying reason might be the extent of the reduction in NO production. Auranofin moderately reduced NO production in RAW 264.7 and Renca but entirely in H6. Auranofin most effectively released the IFN-γ-activated H6 cells from the arrest at S-phase. These support the notion that the regulation and outcome of the IFN-γ-signaling pathway varies between cell types. A detailed mechanism of action study needs to be performed to understand the effects of the compounds on apoptosis.

The IFN-γ activation leads to the promoter occupancy of *Nos2* by STAT1, IRF1, and Interferon stimulated gamma factor (ISGF) 3 complex (comprising STAT1, STAT2, and IRF9), leading to the expression of *Nos2* mRNA. Other transcription factors (such as NF-κB and HIF1α) can also bind the promoter of *Nos2*, synergistically enhancing its transcription [54,55]. Therefore, the regulation of *Nos2* expression is governed by several transcription factors, and the mode of regulation can be context-dependent. In this study, only pentamidine and azithromycin reduced the expression of *Irf1*, one of the transcription factors regulating *Nos2* expression. All the lead compounds reduced *Nos2* expression, where the effect of azithromycin, rolipram, and auranofin was significant. On the other hand, IFN-γ activates the cyclic adenosine monophosphate (cAMP)-pathway, which regulates IFN-γ signaling in PMs [56]. The present study demonstrates that rolipram, a cAMP-elevating agent, further upregulates the NO-independent arms of INF-γ signaling: *Tap2* and *Cd274*. Whether the IFN-γ and cAMP signaling processes synergize at the NO-independent arms remains to be explored. In addition, none of the four leads affected IFN-γ-induced elevation of the MHC Class 1 surface expression in H6 cells, suggesting that the NO-independent processes of the IFN-γ-signaling armamentarium might remain unaffected. Thus, the leads are unlikely to impair the antigen presentation processes and possess broad off-target signal diminution effects. On the other hand, all the leads significantly reduced IFN-γ-induced intracellular accumulation of ROS in H6 cells. Our observations indicate that the leads can protect IFN-γ-stimulated cells from oxidative damage without hampering the endogenous antigen processing and presentation pathway.

Previous studies showed that auranofin inhibits NO production in LPS-stimulated RAW 264.7 macrophages. However, it remained unclear whether auranofin can reduce IFN-γ-induced NO production [57]. Herein, we demonstrate that auranofin effectively inhibited IFN-γ-induced NO production and scored the best goodness of fit in the nonlinear regression analysis of IC_{50} among the hits compared. Auranofin also lowered intracellular ROS in the IFN-γ-activated H6 cells. Although existing literature suggests that auranofin increases intracellular ROS by impairing cellular antioxidant machinery in unstimulated cells [58], it reduced IFN-γ-mediated enhancement of oxidative stress in IFN-γ-activated H6 cells. Rakshit et al demonstrated that IFN-γ-induced NO production is primarily responsible for the increased ROS in the H6 cells [2]. Therefore, the auranofin-mediated interference of IFN-γ-induced *Nos2* expression and subsequent reduction of NO production can be attributed to the reduction in IFN-γ-induced oxidative stress.

IFN-γ-activation-induced M1 polarization of macrophages, and excessive NO production is implicated in several inflammatory diseases, including acute peritonitis and peritonitis sepsis. The activation facilitates the production of several pro-inflammatory cytokines and chemokines. In addition, when mice are exposed to a lethal dosage of LPS, antibody-mediated inhibition of IFN-γ reduces systemic inflammation and increases survival [59]. Herein, we report that auranofin potently reduced IFN-γ-induced NO and IL6 production. Previous reports revealed that auranofin reduces the dimerization of LPS-receptor Toll-like receptor 4 and impairs NF-kB activation in RAW 264.7 macrophage cell line [60,61]. However, the contribution of NF-κB in IFN-γ-inducible NOS2 expression and NO production is minimal in macrophages, whereas the IFN-γ-dependent STAT1α plays an essential role. Erk1/Erk2 contributes to the full activation of STAT1α by mediating STAT1α Ser727 residue phosphorylation in IFN-γ-stimulated macrophages [59]. Whether auranofin can interfere with these kinase functions remains to be investigated. Similar investigations are also required with pentamidine and azithromycin on suppressing IFN-γ-mediated IL6 production.

Inflammatory bowel disease (IBD) refers to two conditions, Crohn's disease, and ulcerative colitis. Both conditions involve chronic digestive

tract inflammation, but they affect different parts of the digestive system. Crohn's disease can affect any part of the digestive tract, from the mouth to the anus. In contrast, ulcerative colitis is usually only in the innermost lining of the large intestine (colon) and rectum [62]. The persistence of ulcerative colitis increases the risk of developing colorectal carcinoma [63]. A study in IBD patients demonstrated that IFN-γ-induced NO pathway plays a pivotal role in ulcerative colitis pathogenesis [12]. Therefore, we expanded the lead evaluation process from *in vitro* tumor cell line and *ex vivo* PMs to *in vivo* disease model of ulcerative colitis to test their efficacy in the body. DSS-mediated experimental ulcerative colitis pathogenesis in mice strongly depends on the elevation of IFN-γ in intestinal tissue and IFN-γ-triggered inflammatory processes [64,65]. Here we demonstrate that *Nos2*$^{-/-}$ mice are protected from DSS-mediated ulcerative colitis in mice. This observation suggests that IFN-γ-induced NOS2 activation might be involved in colitis pathogenesis. Thus, we evaluated the leads in DSS-induced ulcerative colitis in mice. The anti-protozoal drug pentamidine is already reported to ameliorate DSS-induced mouse colitis, likely targeting S100B activity [66]. However, the plan of drug administration was dissimilar. In this comparative study among lead compounds, azithromycin failed to show any significant beneficial effect. This macrolide antibiotic might mechanistically target tumor-specific NO production processes but not in primary cells or *in vivo* disease conditions. Moreover, the gut microbiota plays a protective role in the mouse model of DSS-induced mouse colitis [67]. The antibiotic effects of azithromycin might kill the gut bacteria, leading to the loss of anti-inflammatory functions. Rolipram mildly improved the colon length but could not bring remarkable benefits. Importantly, pentamidine exhibited the best anti-inflammatory effects in ulcerative colitis. Although pentamidine moderately affects IFN-γ-induced NO production *in vitro*, it might target a broad spectrum of pro-inflammatory mediators *in vivo* with efficient bioavailability. Followed by pentamidine, auranofin also remarkably ameliorated ulcerative colitis, as expected from the *in vitro* studies. These effects might be attributed to the auranofin's NF-kB pathway inhibitory property [60,68]. In conclusion, auranofin consistently performed as a potent inhibitor of IFN-γ-induced NO production and in colitis pathogenesis.

Sepsis is a potentially life-threatening medical condition that occurs when the body's response to infection becomes dysregulated and causes inflammation. It is a major concern in hospitals. Globally, 48.9 million sepsis incidences and 11 million deaths occur yearly, accounting for 19.7% of all global deaths [69,70]. It can occur due to any infection, including bacterial, viral, or fungal. The signs of sepsis involve cytokine storm, hemolysis, coagulation, and vascular leakage. A study on the extended prevalence of infection and related sepsis in intensive care unit patients found that 62% of the positive isolates from patients were Gram-negative organisms [71]. Previously, we extensively characterized the effect of NOS2 in a mouse model of the Gram-negative pathogen *Salmonella* Typhimurium infection-induced sepsis. We found that NOS2-induced NO production is essential for the survival of mice [17]. NO is enhanced during sepsis in patients but the effects of NO donors and inhibitors are often inconsistent in clinical reports [18]. In this study, we tested the efficacy of pentamidine and auranofin in a mouse model of the Gram-negative pathogen *Salmonella* Typhimurium infection-induced sepsis. The administration of pentamidine and auranofin was performed 3–4 h post-infection to resemble the clinical scenario. With a single administration, both compounds alleviated sepsis pathogenesis by significantly extending survival. Most likely, the survival of mice in this model is due to the potent anti-inflammatory effects of these two compounds. Many pro-inflammatory cytokines, including IFN-γ *in vivo*, likely contribute to NO production by NOS2 in ulcerative colitis and sepsis [17,25,72]. Our studies involving *Nos2*$^{-/-}$ mice demonstrated that NO production by NOS2 contributes to the disease pathogenesis in DSS-induced ulcerative colitis and *Salmonella* Typhimurium-induced sepsis in mice [Fig.S7; [17,25]. The serum level of IFN-γ increases in both the preclinical mouse disease models [17,25]. Mechanistically, the anti-inflammatory effects of pentamidine and auranofin in ulcerative colitis and sepsis *in vivo* may reduce multiple pro-inflammatory signaling processes. Importantly, pentamidine and auranofin lower inflammatory responses in two distinct mice models of inflammatory disease.

5. Conclusions

The high-throughput screening on IFN-γ-activated H6 cells and the systematic compound validation approach applied and depicted here is paramount in identifying novel and better immunomodulatory drugs targeting many inflammatory diseases. The novel leads identified here against IFN-γ-induced NO production process can be therapeutically repurposed to mitigate adverse inflammatory disease pathogenesis. Furthermore, auranofin and pentamidine may serve as therapeutic options in alternative or combinatorial regimens to treat the chronic inflammatory conditions of inflammatory diseases.

Declaration of Competing Interest

The authors declare that they have no known competing financial interests or personal relationships that could have appeared to influence the work reported in this paper.

Data availability

Data will be made available on request.

Acknowledgments

We greatly appreciate the support from the members of the Divisional flow cytometry facility and Central Animal Facility, IISc. This study was funded by SERB grant CRG/2021/004284, core grants from IISc and the DBT- IISc partnership program. In addition, the infrastructural support from DST-FIST to the Department of Biochemistry, IISc is greatly appreciated. In addition, the support from all members of the laboratory is greatly appreciated.

Appendix A. Supplementary material

Supplementary data to this article can be found online at https://doi.org/10.1016/j.intimp.2023.110569.

References

[1] L.B. Ivashkiv, IFNγ: signalling, epigenetics and roles in immunity, metabolism, disease and cancer immunotherapy, Nat. Rev. Immunol. 18 (2018) 545–558, https://doi.org/10.1038/s41577-018-0029-z.IFN.
[2] S. Rakshit, B.S. Chandrasekar, B. Saha, E.S. Victor, S. Majumdar, D. Nandi, Interferon-gamma induced cell death: regulation and contributions of nitric oxide, cJun N-terminal kinase, reactive oxygen species and peroxynitrite, Biochim. Biophys. Acta - Mol. Cell Res. 2014 (1843) 2645–2661, https://doi.org/10.1016/j.bbamcr.2014.06.014.
[3] L.J. Ignarro, Nitric oxide is not just blowing in the wind, Br. J. Pharmacol. 176 (2019) 131–134, https://doi.org/10.1111/bph.14540.
[4] B. Zhang, W. Crankshaw, R. Nesemeier, J. Patel, I. Nweze, J. Lakshmanan, B. G. Harbrecht, Calcium-mediated signaling and calmodulin-dependent kinase regulate hepatocyte inducible nitric oxide synthase expression, J. Surg. Res. 193 (2015) 795–801, https://doi.org/10.1016/j.jss.2014.07.042.Calcium-mediated.
[5] S. Herbst, U.E. Schaible, B.E. Schneider, Interferon gamma activated macrophages kill mycobacteria by nitric oxide induced apoptosis, PLoS One. 6 (2011), https://doi.org/10.1371/journal.pone.0019105.
[6] J. Braverman, S. Sarah, Nitric oxide modulates macrophage responses to M. tuberculosis infection through activation of HIF-1α and repression of NF-kB, Physiol. Behav. 176 (2019) 139–148, https://doi.org/10.4049/jimmunol.1700515.Nitric.
[7] G. Kak, M. Raza, B.K. Tiwari, Interferon-gamma (IFN-γ): exploring its implications in infectious diseases, Biomol. Concepts. 9 (2018) 64–79, https://doi.org/10.1515/bmc-2018-0007.
[8] B. Saha, S.J. Prasanna, B.S. Chandrasekar, D. Nandi, Gene modulation and immunoregulatory roles of Interferonγ, Cytokine. 50 (2010) 1–14, https://doi.org/10.1016/j.cyto.2009.11.021.

[9] S. Ambs, W.G. Merriam, W.P. Bennet, E. Felley-Bosco, M.O. Ogunfusika, S.M. Oser, S. Klein, P.G. Shields, T.R. Billiar, C.C. Harris, Frequent Nitric oxide synthase-2 expression in human colon adenomas: implication for tumor angiogenesis and colon cancer progression, Cancer Res. 58 (1998) 334–341.
[10] H. Okayama, M. Saito, N. Oue, J.M. Weiss, J. Stauffer, S. Takenoshita, R. H. Wiltrout, S.P. Hussain, C.C. Harris, NOS2 enhances KRAS-induced lung carcinogenesis, inflammation and microRNA-21 expression, Int. J. Cancer. 132 (2013) 9–18, https://doi.org/10.1002/ijc.27644.
[11] S. Granados-Principal, Y. Liu, M.L. Guevara, E. Blanco, D.S. Choi, W. Qian, T. Patel, A.A. Rodriguez, J. Cusimano, H.L. Weiss, H. Zhao, M.D. Landis, B. Dave, S.S. Gross, J.C. Chang, Inhibition of iNOS as a novel effective targeted therapy against triple-negative breast cancer, Breast Cancer Res. 17 (2015) 1–16, https://doi.org/10.1186/s13058-015-0527-x.
[12] H. Rafa, M. Amri, H. Saoula, M. Belkhelfa, O. Medjeber, A. Boutaleb, S. Aftis, M. Nakmouche, C. Touil-Boukoffa, Involvement of interferon-γ in bowel disease pathogenesis by nitric oxide pathway: a study in algerian patients, J. Interf. Cytokine Res. 30 (2010) 691–697, https://doi.org/10.1089/jir.2010.0012.
[13] G. Arellano, P.A. Ottum, L.I. Reyes, P.I. Burgos, R. Naves, Stage-specific role of interferon-gamma in experimental autoimmune encephalomyelitis and multiple sclerosis, Front. Immunol. 6 (2015), https://doi.org/10.3389/fimmu.2015.00492.
[14] S. Benchabane, A. Boudjelida, R. Toumi, H. Belguendouz, P. Youinou, C. Touil-Boukoffa, A case for IL-6, IL-17A, and nitric oxide in the pathophysiology of Sjögren's syndrome, Int. J. Immunopathol. Pharmacol. 29 (2016) 386–397, https://doi.org/10.1177/0394632016651273.
[15] P. Dey, V. Panga, S. Raghunathan, A cytokine signalling network for the regulation of inducible nitric oxide synthase expression in rheumatoid arthritis, PLoS One. 11 (2016) 1–29, https://doi.org/10.1371/journal.pone.0161306.
[16] W. Liu, S. Zhang, J. Wang, IFN-γ, should not be ignored in SLE, Front. Immunol. 13 (2022) 1–10, https://doi.org/10.3389/fimmu.2022.954706.
[17] S. Yadav, S. Pathak, M. Sarikhani, S. Majumdar, S. Ray, B.S. Chandrasekar, V. Adiga, N.R. Sundaresan, D. Nandi, Nitric oxide synthase 2 enhances the survival of mice during Salmonella Typhimurium infection-induced sepsis by increasing reactive oxygen species, inflammatory cytokines and recruitment of neutrophils to the peritoneal cavity, Free Radic. Biol. Med. 116 (2018) 73–87, https://doi.org/10.1016/j.freeradbiomed.2017.12.032.
[18] S. Yadav, T. Verma, S. Pathak, D. Nandi, "Understanding the roles of nitric oxide during sepsis, an inflammatory disorder," in Therapeutic applications of nitric oxide in cancer and inflammatory disorders (2019), chapter 13, pages 243-276, editors Benjamin Bonavida and Lucia Morbidelli published by Elsevier. https://doi.org/10.1016/B978-0-12-816545-4.00013-X.
[19] E. Coates, A. Barr, N. Totton, D. Hind, P. Shackley, S. Blackwell, N. Dames, H. Bedford, M. Lee, S. Sebastian, C. Probert, A. Lobo, P97 Management of steroid resistant ulcerative colitis – a national survey of UK practice, Gut. 70 (2021) A1–A262.
[20] T.D. Warner, S.A. McCartney, NOS inhibitors in colitis: a suitable case for treatment? Gut. 42 (1998) 152–153, https://doi.org/10.1136/gut.42.2.152.
[21] S.J. Prasanna, B. Saha, D. Nandi, Involvement of oxidative and nitrosative stress in modulation of gene expression and functional responses by IFNγ, Int. Immunol. 19 (2007) 867–879, https://doi.org/10.1093/intimm/dxm058.
[22] BS Chandrasekar, S Yadav, ES Victor, S Majumdar, M Deobagkar-Lele, N Wadhwa, S Podder, M Das, D Nandi, Interferon-Gamma and Nitric Oxide Synthase 2 Mediate the Aggregation of Resident Adherent Peritoneal Exudate Cells: Implications for the Host Response to Pathogens (2015) PLoS One https://doi.org/10.1371/journal.pone.0128301.
[23] S. Malu, S. Srinivasan, P.K. Maiti, D. Rajagopal, B. John, D. Nandi, IFN-γ bioassay: development of a sensitive method by measuring nitric oxide production by peritoneal exudate cells from C57BL/6 mice, J. immunological methods 272 (2003) 55–65, https://doi.org/10.1016/S0022-1759(02)00424-6.
[24] E.E. Bou Ghosn, A.A. Cassado, G.R. Govoni, T. Fukuhara, Y. Yang, D.M. Monack, K. R. Bortoluci, S.R. Almeida, L.A. Herzenberg, L.A. Herzenberg, Two physically, functionally, and developmentally distinct peritoneal macrophage subsets, Proc. Natl. Acad. Sci. U. S. A. 107 (2010) 2568–2573, https://doi.org/10.1073/pnas.0915000107.
[25] S. Pathak, A. Gokhroo, A. Kumar Dubey, S. Majumdar, S. Gupta, A. Almeida, G. B. Mahajan, A. Kate, P. Mishra, R. Sharma, S. Kumar, R. Vishwakarma, A. Balakrishnan, H. Atreya, D. Nandi, 7-Hydroxy Frullanolide, a sesquiterpene lactone, increases intracellular calcium amounts, lowers CD4+ T cell and macrophage responses, and ameliorates DSS-induced colitis, Int. Immunopharmacol. 97 (2021), 107655, https://doi.org/10.1016/j.intimp.2021.107655.
[26] Y.H. Park, N. Kim, Y.K. Shim, Y.J. Choi, R.H. Nam, Y.J. Choi, M.H. Ham, J.H. Suh, S.M. Lee, C.M. Lee, H. Yoon, H.S. Lee, D.H. Lee, Adequate dextran sodium sulfate-induced colitis model in mice and effective outcome measurement method, J Cancer Prevention 20 (2015) 260–267, https://doi.org/10.15430/JCP.2015.20.4.260.
[27] A. Chattopadhyay, J.P. Joseph, S. Shyam, D. Nandi, Characterizing salmonella typhimurium-induced septic peritonitis in mice, J. Vis. Exp. 185 (2022), https://doi.org/10.3791/63695-v.
[28] J.H. Zhang, T.D.Y. Chung, K.R. Oldenburg, A simple statistical parameter for use in evaluation and validation of high throughput screening assays, J. Biomol. Screen. 4 (1999) 67–73, https://doi.org/10.1177/108705719900400206.
[29] X. Hu, W.-P. Li, C. Meng, L.B. Ivashkiv, Inhibition of IFN-γ Signaling by Glucocorticoids, J. Immunol. 170 (2003) 4833–4839, https://doi.org/10.4049/jimmunol.170.9.4833.
[30] P.J. Barnes, How corticosteroids control inflammation: quintiles prize lecture 2005, Br. J. Pharmacol. 148 (2006) 245–254, https://doi.org/10.1038/sj.bjp.0706736.
[31] J. Blanchette, M. Jaramillo, M. Olivier, Signaling events involved in interferon-γ-inducible macrophage nitric oxide generation, Immunology. 108 (2003) 513–522, https://doi.org/10.1046/j.1365-2567.2003.01620.x.
[32] E. Martin, C. Nathan, Q.W. Xie, Role of interferon regulatory factor 1 in induction of nitric oxide synthase, J. Exp. Med. 180 (1994) 977–984, https://doi.org/10.1084/jem.180.3.977.
[33] C.M. Zajd, A.M. Ziemba, G.M. Miralles, T. Nguyen, P.J. Feustel, S.M. Dunn, R. J. Gilbert, M.R. Lennartz, Bone marrow-derived and elicited peritoneal macrophages are not created equal: the questions asked dictate the cell type used, Front. Immunol. 11 (2020) 1–19, https://doi.org/10.3389/fimmu.2020.00269.
[34] E. Antoniou, G.A. Margonis, A. Angelou, A. Pikouli, P. Argiri, I. Karavokyros, A. Papalois, E. Pikoulis, The TNBS-induced colitis animal model: an overview, Ann. Med. Surg. 11 (2016) 9–15.
[35] G.R. Jones, C.C. Bain, T.M. Fenton, A. Kelly, S.L. Brown, A.C. Ivens, M.A. Travis, P. C. Cook, A.S. MacDonald, Dynamics of colon monocyte and macrophage activation during colitis, Front. Immunol. 9 (2018), https://doi.org/10.3389/fimmu.2018.02764.
[36] N. Shintani, T. Nakajima, T. Okamoto, T. Kondo, N. Nakamura, T. Mayumi, Involvement of CD4+ T cells in the development of dextran sulfate sodium-induced experimental colitis and suppressive effect of IgG on their action, Gen. Pharmacol. 31 (1998) 477–481, https://doi.org/10.1016/S0306-3623(98)00004-4.
[37] F.R. Salamone, B.A. Cunha, Update on pentamidine for the treatment of Pneumocystis carinii pneumonia, Clin Pharm 7 (1988) 501–510. PMID: 3046830.
[38] T. Sun, Y. Zhang, Pentamidine binds to tRNA through non-specific hydrophobic interactions and inhibits aminoacylation and translation, Nucleic Acids Res. 36 (2008) 1654–1664, https://doi.org/10.1093/nar/gkm1180.
[39] J. Sultana, P.M. Cutroneo, S. Crisafulli, G. Puglisi, G. Caramori, G. Trifirò, Azithromycin in COVID-19 patients: pharmacological mechanism, clinical evidence and prescribing guidelines, Drug Saf. 43 (2020) 691–698, https://doi.org/10.1007/s40264-020-00976-7.
[40] N. Principi, F. Blasi, S. Esposito, Azithromycin use in patients with cystic fibrosis, Eur. J. Clin. Microbiol. Infectious Dis. 34 (2015) 1071–1079, https://doi.org/10.1007/s10096-015-2347-4.
[41] H. Huang, M. Xie, L. Gao, W. Zhang, X. Zhu, Y. Wang, W. Li, R. Wang, K. Chen, M. Boutjdir, L. Chen, Rolipram, a PDE4 inhibitor, enhances the inotropic effect of rat heart by activating SERCA2a, Front. Pharmacol. 10 (2019), https://doi.org/10.3389/fphar.2019.00221.
[42] X. Zhang, K. Selvaraju, A.A. Saei, P. D'Arcy, R.A. Zubarev, E.S. Arnér, S. Linder, Repurposing of auranofin: thioredoxin reductase remains a primary target of the drug, Biochimie. 162 (2019) 46–54, https://doi.org/10.1016/j.biochi.2019.03.015.
[43] C. Roder, M.J. Thomson, Auranofin: repurposing an old drug for a golden new age, Drugs R D. 15 (2015) 13–20, https://doi.org/10.1007/s40268-015-0083-y.
[44] T. Doan, E. Massarotti, Rheumatoid arthritis: an overview of new and emerging therapies, J. Clin. Pharmacol. 45 (2005) 751–762, https://doi.org/10.1177/0091270005277938.
[45] M. Gil-Moles, U. Basu, R. Büssing, H. Hoffmeister, S. Türck, A. Varchmin, I. Ott, Gold metallodrugs to target coronavirus proteins: inhibitory effects on the spike-ACE2 interaction and on PLpro protease activity by auranofin and gold organometallics**, Chem. - A Eur. J. 26 (2020) 15140–15144, https://doi.org/10.1002/chem.202004112.
[46] E. Laplantine, C. Chable-Bessia, A. Oudin, J. Swain, A. Soria, P. Merida, M. Gourdelier, S. Mestiri, I. Besseghe, E. Bremaud, A. Neyret, S. Lyonnais, C. Favard, P. Benaroch, M. Hubert, O. Schwartz, M. Guerin, A. Danckaert, E. Del Nery, D. Muriaux, R. Weil, The FDA-approved drug Auranofin has a dual inhibitory effect on SARS-CoV-2 entry and NF-κB signaling, IScience. 25 (2022), https://doi.org/10.1016/j.isci.2022.105066.
[47] J.M. Madeira, C.J. Renschler, B. Mueller, S. Hashioka, D.L. Gibson, A. Klegeris, Novel protective properties of auranofin: inhibition of human astrocyte cytotoxic secretions and direct neuroprotection, Life Sci. 92 (2013) 1072–1080, https://doi.org/10.1016/j.lfs.2013.04.005.
[48] K.P. Kotredes, A.M. Gamero, Interferons as inducers of apoptosis in malignant cells, J. Interf. Cytokine Res. 33 (2013) 162–170, https://doi.org/10.1089/jir.2012.0110.
[49] S.H. Lee, J.Y. Kwon, S.Y. Kim, K.A. Jung, M. La Cho, Interferon-gamma regulates inflammatory cell death by targeting necroptosis in experimental autoimmune arthritis, Sci. Rep. 7 (2017) 2–10, https://doi.org/10.1038/s41598-017-09767-0.
[50] Q. Su, F. Wang, Z. Dong, M. Chen, R. Cao, IFN γ induces apoptosis in human melanocytes by activating the JAK1/STAT1 signaling pathway, Mol. Med. Rep. 22 (2020) 3111–3116, https://doi.org/10.3892/mmr.2020.11403.
[51] O. Kann, F. Almouhanna, B. Chausse, Interferon γ: a master cytokine in microglia-mediated neural network dysfunction and neurodegeneration, Trends Neurosci. 45 (2022) 913–927, https://doi.org/10.1016/j.tins.2022.10.007.
[52] E. Alspach, D.M. Lussier, R.D. Schreiber, Interferon γ and its important roles in promoting and inhibiting spontaneous and therapeutic cancer immunity, Cold Spring Harb. Perspect. Biol. 11 (2019), a028480, https://doi.org/10.1101/cshperspect.a028480.
[53] J. Gao, L.Z. Shi, H. Zhao, J. Chen, L. Xiong, Q. He, T. Chen, J. Roszik, C. Bernatchez, S.E. Woodman, P.L. Chen, P. Hwu, J.P. Allison, A. Futreal, J. A. Wargo, P. Sharma, Loss of IFN-γ pathway genes in tumor cells as a mechanism of resistance to Anti-CTLA-4 Therapy, Cell. 167 (2016) 397–404.e9, https://doi.org/10.1016/j.cell.2016.08.069.

[54] H. Kleinert, J. Art, A. Pautz, Regulation of the expression of inducible nitric oxide synthase, Nitric Oxide. 384 (2010) 211–267, https://doi.org/10.1016/B978-0-12-373866-0.00007-1.
[55] C. Bogdan, Nitric oxide synthase in innate and adaptive immunity: an update, Trends Immunol. 36 (2015) 161–178, https://doi.org/10.1016/j.it.2015.01.003.
[56] L. Liu, Y. Wang, Y. Fan, C.L. Li, Z.L. Chang, IFN-γ activates cAMP/PKA/CREB signaling pathway in murine peritoneal macrophages, J. Interf. Cytokine Res. 24 (2004) 334–342, https://doi.org/10.1089/107999004323142196.
[57] S. Han, K. Kim, H. Kim, J. Kwon, Y.H. Lee, C.K. Lee, Y. Song, S.J. Lee, N. Ha, K. Kim, Auranofin inhibits overproduction of pro-inflammatory cytokines, cyclooxygenase expression and PGE2 production in macrophages, Arch. Pharm. Res. 31 (2008) 67–74, https://doi.org/10.1007/s12272-008-1122-9.
[58] P. Zou, M. Chen, J. Ji, W. Chen, X. Chen, S. Ying, J. Zhang, Z. Zhang, Z. Liu, S. Yang, G. Liang, Auranofin induces apoptosis by ROS-mediated ER stress and mitochondrial dysfunction and displayed synergistic lethality with piperlongumine in gastric cancer, Oncotarget. 6 (2015) 36505–36521, https://doi.org/10.18632/oncotarget.5364.
[59] C.R. Romero, D.S. Herzig, A. Etogo, J. Nunez, R. Mahmoudizad, G. Fang, E. D. Murphey, T. Toliver-Kinsky, E.R. Sherwood, The role of interferon-γ in the pathogenesis of acute intra-abdominal sepsis, J. Leukoc. Biol. 88 (2010) 725–735, https://doi.org/10.1189/jlb.0509307.
[60] H. Hwangbo, S.Y. Ji, M.Y. Kim, S.Y. Kim, H. Lee, G.Y. Kim, S. Kim, J. Cheong, Y. H. Choi, Anti-inflammatory effect of auranofin on palmitic acid and lps-induced inflammatory response by modulating tlr4 and nox4-mediated nf-κb signaling pathway in raw264.7 macrophages, Int. J. Mol. Sci. 22 (2021) 1–17, https://doi.org/10.3390/ijms22115920.
[61] H.S. Youn, J.Y. Lee, S.I. Saitoh, K. Miyake, D.H. Hwang, Auranofin, as an anti-rheumatic gold compound, suppresses LPS-induced homodimerization of TLR4, Biochem. Biophys. Res. Commun. 350 (2006) 866–871, https://doi.org/10.1016/j.bbrc.2006.09.097.
[62] D.C. Baumgart, S.R. Carding, Inflammatory bowel disease: cause and immunobiology, Lancet. 369 (2007) 1627–1640.
[63] P.L. Lakatos, L. Lakatos, Risk for colorectal cancer in ulcerative colitis: changes, causes and management strategies, World J. Gastroenterol. 14 (2008) 3937–3947, https://doi.org/10.3748/wjg.14.3937.
[64] R. Ito, M. Shin-Ya, T. Kishida, A. Urano, R. Takada, J. Sakagami, J. Imanishi, M. Kita, Y. Ueda, Y. Iwakura, K. Kataoka, T. Okanoue, O. Mazda, Interferon-gamma is causatively involved in experimental inflammatory bowel disease in mice, Clin. Exp. Immunol. 146 (2006) 330–338, https://doi.org/10.1111/j.1365-2249.2006.03214.x.
[65] V. Langer, E. Vivi, D. Regensburger, T.H. Winkler, M.J. Waldner, T. Rath, B. Schmid, L. Skottke, S. Lee, N.L. Jeon, T. Wohlfahrt, V. Kramer, P. Tripal, M. Schumann, S. Kersting, C. Handtrack, C.I. Geppert, K. Suchowski, R.H. Adams, C. Becker, A. Ramming, E. Naschberger, N. Britzen-Laurent, M. Stürzl, IFN-γ drives inflammatory bowel disease pathogenesis through VE-cadherin–directed vascular barrier disruption, J. Clin. Invest. 129 (2019) 4691–4707, https://doi.org/10.1172/JCI124884.
[66] G. Esposito, E. Capoccia, G. Sarnelli, C. Scuderi, C. Cirillo, R. Cuomo, L. Steardo, The antiprotozoal drug pentamidine ameliorates experimentally induced acute colitis in mice, J. Neuroinflammation. 9 (2012) 1–12, https://doi.org/10.1186/1742-2094-9-277.
[67] A. Le Bras, Gut microbiota drives disease variability in the DSS colitis mouse model, Lab Anim (NY) 51 (2022) 128, https://doi.org/10.1038/s41684-022-00967-4.
[68] I. Atreya, R. Atreya, M.F. Neurath, NF-κB in inflammatory bowel disease, J. Intern. Med. 263 (2008) 591–596, https://doi.org/10.1111/j.1365-2796.2008.01953.x.
[69] R.S. Hotchkiss, L.L. Moldawer, S.M. Opal, K. Reinhart, I.R. Turnbull, J.L. Vincent, Sepsis and septic shock, Nat. Rev. Dis. primers 2 (1) (2016) 1–21, https://doi.org/10.1038/nrdp.2016.45.
[70] K.E. Rudd, S.C. Johnson, K.M. Agesa, K.A. Shackelford, D. Tsoi, D.R. Kievlan, M. Naghavi, Global, regional, and national sepsis incidence and mortality, 1990–2017: analysis for the Global Burden of Disease Study, The Lancet 395 (10219) (2020) 200–211, https://doi.org/10.1016/S0140-6736(19)32989-7.
[71] J.L. Vincent, J. Rello, J. Marshall, E. Silva, A. Anzueto, C.D. Martin, Epic II Group of Investigators International study of the prevalence and outcomes of infection in intensive care units, Jama 302 (21) (2009) 2323–2329, https://doi.org/10.1001/jama.2009.1754.
[72] I. Soufli, R. Toumi, H. Rafa, Touil-Boukoffa, C, Overview of cytokines and nitric oxide involvement in immuno-pathogenesis of inflammatory bowel diseases, World J. Gastrointest. Pharmacol. Ther. 7 (2016) 353, https://doi.org/10.4292/wjgpt.v7.i3.353.

jove

Characterizing *Salmonella* Typhimurium-induced Septic Peritonitis in Mice

Avik Chattopadhyay[1], **Joel P. Joseph**[2], **Sai Shyam**[3], **Dipankar Nandi**[1]

[1] Department of Biochemistry, Indian Institute of Science [2] Center for BioSystems Science and Engineering, Indian Institute of Science [3] Undergraduate Program, Indian Institute of Science

Corresponding Author

Dipankar Nandi
nandi@iisc.ac.in

Citation

Chattopadhyay, A., Joseph, J.P., Shyam, S., Nandi, D. Characterizing *Salmonella* Typhimurium-induced Septic Peritonitis in Mice. *J. Vis. Exp.* (185), e63695, doi:10.3791/63695 (2022).

Date Published

July 29, 2022

DOI

10.3791/63695

URL

jove.com/video/63695

Abstract

Sepsis is a dysregulated host immune response to microbial invasion or tissue damage, leading to organ injury at a site distant from that of the infection or damage. Currently, the widely used mice models of sepsis include lipopolysaccharide (LPS)-induced endotoxemia, cecal ligation and puncture (CLP), and monobacterial infection model systems. This protocol describes a method to study the host responses during *Salmonella* Typhimurium infection-induced septic peritonitis in mice. *S.* Typhimurium, a Gram-negative intracellular pathogen, causes typhoid-like disease in mice.

This protocol elaborates the culture preparation, induction of septic peritonitis in mice through intraperitoneal injection, and methods to study systemic host responses. Furthermore, the assessment of bacterial burden in different organs and the flow cytometric analysis of increased neutrophil numbers in the peritoneal lavage is presented. *Salmonella* Typhimurium-induced sepsis in mice leads to an increase in proinflammatory cytokines and rapid infiltration of neutrophils in the peritoneal cavity, leading to lower survival.

Every step in this protocol has been optimized, resulting in high reproducibility of the pathogenesis of septic peritonitis. This model is useful for studying immunological responses during bacterial sepsis, the roles of different genes in disease progression, and the effects of drugs to attenuate sepsis.

Introduction

Sepsis is defined as a dysregulated systemic inflammatory and immune response to microbial invasion or tissue damage, leading to organ injury distant from the site of infection or damage. Septic shock is a subset of sepsis characterized by hypotension persisting during volume resuscitation, with a substantially increased risk of mortality[1]. The general public has become more aware of this disorder during the COVID-19 pandemic. Despite its high associated mortality,

comprehensive epidemiological data on the global burden of sepsis is lacking because of the complexity of its diagnosis. In 2017, there were 48.9 million sepsis incidences and 11 million deaths worldwide, accounting for 19.7% of all global deaths[2]. Further, a study on the extended prevalence of infection and related sepsis in intensive care unit patients found that 62% of the positive isolates from patients were Gram-negative organisms[3].

Initially, the investigations on sepsis focused on delineating microbial pathogenesis. However, understanding the "danger hypothesis", which dictates how the host distinguishes self and non-self, led to the tilting of the balance of sepsis research toward understanding the host response to an invading pathogen. The widely used mice models of sepsis include the lipopolysaccharide (LPS)-induced endotoxemia model, polymicrobial sepsis models, cecal ligation and puncture (CLP) and colon ascendens stent peritonitis (CASP), and monobacterial infection models[4].

We have standardized a mouse model system by inducing peritoneal sepsis using *Salmonella* Typhimurium. This model is advantageous over others because *Salmonella* Typhimurium is an intracellular pathogen that mimics the clinically relevant condition of Gram-negative sepsis. The outcome of peritonitis sepsis in this model is systemic, with 100% mortality within 96 h post infection. Therefore, this model is instrumental in studying the inflammatory and lethal host responses. In this model, sepsis is induced by intraperitoneally injecting 0.5 million colony-forming units (CFU) of *Salmonella* Typhimurium into an 8-10-week-old C57BL/6 mouse. Systemic infection can be confirmed by assessing organ bacterial burden ~16 h post infection. This article demonstrates *Salmonella* Typhimurium-induced peritonitis sepsis in mice, characterizes the resulting alterations in peritoneal cell composition, and quantifies bacterial burden in different organs.

Protocol

All experiments using *Salmonella* Typhimurium were conducted in Bio Safety Level 2 (BSL-2) facilities. Care must be taken to use proper personal protective equipment (PPE), ensure safety, and follow standard BSL-2 biohazard disposal methods. All mice experiments were conducted following guidelines stated by the Institutional Animal Ethics Committee, IISc. Mice were bred and maintained at the Central Animal Facility of IISc (Registration number: 48/1999/CPCSEA, dated 1/3/1999), approved by the Ministry of Environment and Forest, Government of India. The experimental protocols were approved by the Committee for Purpose and Control and Supervision of Experiments on Animals with the approved permit number CAF/Ethics/797/2020.

BSL2 definition: A BSL2 rating represents that the biohazardous agents pose a moderate threat to the environment and laboratory staff[5].

1. Culture preparation of *Salmonella* Typhimurium

1. Add 100 µL of *Salmonella* Typhimurium NCTC 12023 glycerol stock to 3 mL of Luria Bertani (LB) broth. Incubate the culture at 160 rpm at 37 °C overnight.
2. Streak 50 µL of the overnight grown culture in LB broth onto a Salmonella Shigella (SS) agar plate and incubate at 37 °C for ~12 h. Store the SS agar plate with the bacterial colonies at 4 °C for several days before the *in vivo* infection experiment.

3. Pick a single colony from the streaked SS agar plate using a microtip. Eject the microtip into 3 mL of LB broth and culture at 160 rpm at 37 °C overnight.

4. Add 0.1 mL of the bacterial culture to 50 mL of LB broth and incubate at 37 °C in a shaker incubator at 160 rpm for 3-4 h to reach the logarithmic phase of growth. Dilute the culture by a factor of 2 using LB broth.
   NOTE: During the logarithmic phase, bacterial cells are at their best health and are actively dividing.

5. Measure the optical density (OD) of the culture at 600 nm wavelength of light in a spectrophotometer or microplate reader. Once the OD reaches 1.0, make two aliquots of 1 mL of culture in 1.5 mL microfuge tubes.

6. Centrifuge the tubes at 7,750 × *g* for 15 min. Discard the supernatant and wash the pellet with 1 mL of 1x PBS 2x. Centrifuge the tubes at 7,750 × *g* for 15 min.

7. Resuspend the pellet in 0.5 mL of 1x PBS in two different 1.5 mL microfuge tubes. Combine the suspensions from both the tubes into one 1.5 mL tube now containing ~2 × 10^8 colony-forming units (CFU)/mL.

8. Prepare a bacterial cell suspension of 1 × 10^6 CFU/mL by diluting this stock solution.
   CAUTION: Optimize the CFU corresponding to OD under specific laboratory conditions to determine the CFU for OD 1.0 before initiating the experiments.

2. Mice and infections

1. House 8-10-week-old male C57BL/6 mice weighing ~20 g in the clean-air room of the animal facility for several days for acclimation.

2. On the day of infection, hold the mouse with one hand, wipe the abdominal skin with 70% ethanol, and spread the hind legs for better accessibility of the abdominal wall.

3. Inject 0.5 mL of 1 × 10^6 CFU/mL bacterial suspension intraperitoneally with the help of a 1 mL syringe. Therefore, each mouse receives 5 × 10^5 CFU. Control, uninfected mice receive 0.5 mL of PBS alone. Post infection, plate the culture to check the actual CFU injected, which may vary from 0.2-0.8 million CFU/0.5 mL.

4. Put the mice back in the cages as assigned.

5. Sacrifice the mice using CO_2 asphyxiation ~12-18 h post infection for the best response. Usually, all infected mice die within 96 h. Under some experimental interventions, some mice may survive. Euthanize these mice after 96 h. Also, euthanize any mouse with a body temperature below 33.2 °C and acute distress at 96 h as a humane endpoint.
   NOTE: In this model, some mice may start dying after 12 h of *Salmonella* injection. Therefore, plan experiments properly involving multiple time points.

3. CFU assessment of organs

1. Sacrifice the infected mouse by CO_2 asphyxiation, and wipe the abdomen with a piece of cotton dipped in 70% ethanol. Cut open the abdominal skin. Refer to the article by Ray and Dittel for a video protocol on how to collect peritoneal lavage fluid[6]. Cut open the peritoneal cavity and collect the organs of interest in microfuge tubes. Additionally, as the blood in mice with sepsis gets coagulated fast and the amounts are low, collect it quickly after sacrificing.

NOTE: This video demonstrates the enumeration of organ CFU from the liver as the liver undergoes extensive histopathological damage in this model of sepsis.

2. Cut a small piece of the liver and place it in a microfuge tube.

   NOTE: This can be stored on ice for a maximum of 2-3 h before proceeding to the next step.

3. Weigh and transfer the pieces to microcentrifuge tubes. Preferably, cut pieces weighing ~10-15 mg for proper homogenization. Use entire organs in the case of smaller ones such as the mesenteric lymph nodes (MLNs) or thymus.

4. Add 0.5 mL of 1x PBS to the tube and homogenize the organs using a hand homogenizer. Make sure that the organs are completely homogenized. Make up the volume to 1 mL by adding 0.5 mL of 1x PBS.

5. Centrifuge the tubes at 200 × *g* for 5 min at 4 °C.

6. Collect the supernatant into fresh microfuge tubes and prepare dilutions of 1×10^{-1} and 10^{-2} in a 96-well plate.

7. Spread 50 µL of the diluent onto fresh SS agar plates and incubate the plates at 37 °C for 12 h.

8. Count the number of colonies that appear in each condition and normalize the data with the organ weight using Equation (**1**):

$$\text{CFU/mg} = \frac{\text{Number of colonies} \times 20 \times \text{Dilution factor}}{\text{Organ weight in mg}} \quad (1)$$

   NOTE: The number 20 is used in the formula to convert the colonies per plate to CFU/mL. This number is arrived at by dividing 1 mL by the amount of a given volume of the culture plated-in this case, 50 µL.

   For example, if 100 colonies are found in an SS agar plate, where 50 µL of a 1×10^{-1} dilution of a homogenized organ weighing 10 mg is spread, then

$$\text{CFU/mg} = \frac{100 \times 20 \times 10}{10} = 2{,}000$$

4. Flow cytometric analysis of various immune cell populations in peritoneal exudate

1. Collect the peritoneal cells as described previously by Ray and Dittel[6].

2. Resuspend the cell pellet from peritoneal lavage fluid in 1 mL of RPMI supplemented with 10% fetal bovine serum (FBS). Enumerate the total cell numbers in the peritoneal lavage using a hemocytometer. Adjust the cell number so that every tube receives 0.2-0.5 million cells.

   NOTE: Peritoneal lavage in mice with sepsis may contain RBCs, which probably appear due to hemorrhage. Be careful to exclude RBCs while counting peritoneal cells. In the brightfield microscope, RBCs appear much smaller than the immune cells. These appear as flat disks or doughnuts, round, with an indentation in the center, but not hollow. A step to lyse RBCs may be added[7].

3. Spin the cells down at 200 × *g* at 4 °C for 10 min, discard the supernatant, and wash the cells 1x with 1x cold PBS. Centrifuge the cells at 200 × *g* at 4 °C for 10 min.

4. Block the Fc receptors on PECs using FcR blocker (1:400 dilution), prepared in blocking buffer consisting of 5% FBS and 0.02% sodium azide in PBS. Incubate on ice for 15 min.

5. Centrifuge the cells at 200 × *g* at 4 °C for 10 min. Discard the supernatant. Dilute the fluorochrome-conjugated antibodies of interest in blocking buffer. Use a 1:500 dilution of anti-mouse LY6G to stain the neutrophils.

NOTE: Other immune cell populations can also be detected using, for example, anti-mouse B220 for B cells, anti-mouse CD3 for T cells, and anti-mouse F4/80 for macrophages.

6. Incubate ~0.2 million cells in 200 µL of the diluted solutions of antibodies in separate tubes. As a negative control, set aside one tube in each fluorochrome type for the unstained control to incubate the cells with 200 µL of blocking buffer without antibody.

7. Incubate the samples on ice for 45 min with intermittent tapping every 15 min.

8. Centrifuge the cells at 200 × *g* for 10 min at 4 °C. Discard the supernatant. Fix the cells with 4% paraformaldehyde for ~15 min at room temperature if they need to be be stored for several days. However, it is best to acquire data from freshly stained samples in a flow cytometer.

9. Resuspend the cells in 200 µL of FACS staining buffer (2% FBS in PBS). Acquire the data in a flow cytometer.

Representative Results

A detailed characterization of the host immune response using this particular model is shown in previous publications[8,9]. A few representative results of the described protocol are depicted in this section. This model aims to induce systemic infection of *S.* Typhimurium by intraperitoneal injection of the bacterial culture to induce sepsis. To confirm the infection, the lysates of the liver and spleen from septic mice were spread on SS agar plates, and the number of colonies was counted. In **Figure 1**, the images of SS agar plates indicate the organ CFU burden in the liver and spleen of septic mice. The homogenized organ lysates were spread at a dilution of 1×10^{-1} and incubated at 37 °C. The black pigmented *S.* Typhimurium colonies appeared after ~12 h of incubation at 37 °C. Furthermore, upon infection of mice, the cultures from blood and peritoneal lavage are reported to be positive for bacterial cells[8]. These results indicated that the intraperitoneally injected bacterial cells disseminated systemically and colonized the internal organs. A part of the plate is shown as a zoomed-in inset to highlight the colonies. The pathogen successfully disseminated systemically and colonized the internal organs.

Figure 2 shows the sera isolated from healthy and septic mice. The volume of collectible blood through cardiac puncture from septic mice is usually 100-200 µL, which is lower than the amount from healthy mice, where ~500 µL of blood can be obtained. As a result, the serum volume isolated from septic mouse blood is low. This phenomenon happens because of the increased coagulation of the blood in septic mice. Moreover, the sera from septic mice show distinct red coloration, indicating the occurrence of extensive hemolysis[8,9].

As shown in **Figure 3**, flow cytometry-based immunophenotyping of peritoneal exudate cells was performed to assess the infiltration of neutrophils in the peritoneal cavity of healthy and septic mice. As neutrophils express LY6G protein on the cell surface, FITC-tagged anti-LY6G antibody was used to stain the neutrophil cell population. These images represent data from one healthy and two infected mice. After data acquisition, the cells were gated to include only singlets in an FSC-A versus SSC-A plot. Then, the histogram plots and dot-plot were drawn. Here, the septic mice showed increased infiltration of neutrophils in the peritoneal cavity.

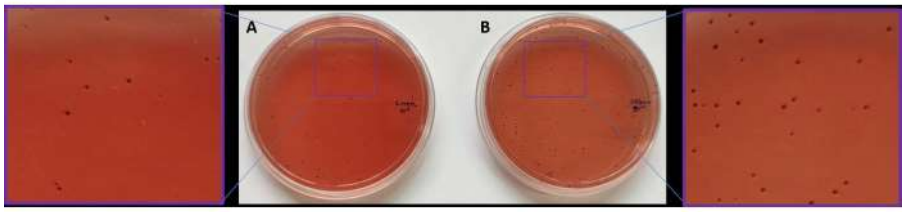

Figure 1: Visualization of organ CFU post infection. Organs were homogenized as described in the protocol. The lysate was spread on SS agar plates using a spreader. Images of plates spread with a 1×10^{-1} dilution of homogenized lysates of (**A**) liver and (**B**) spleen. A part of the plate is shown as a zoomed inset to highlight the colonies. Inset magnification = 13x (area). Please click here to view a larger version of this figure.

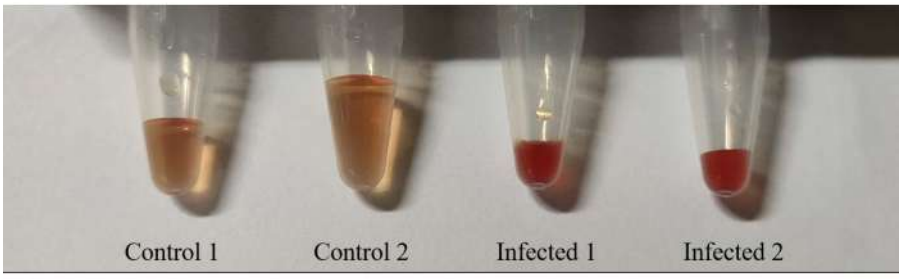

Figure 2: Enhanced hemolysis in septic mice. The blood was collected in microcentrifuge tubes and left undisturbed at room temperature for 30 min. The clot was removed by centrifuging the tubes at 2,000 × *g* for 10 min in a refrigerated centrifuge. Please click here to view a larger version of this figure.

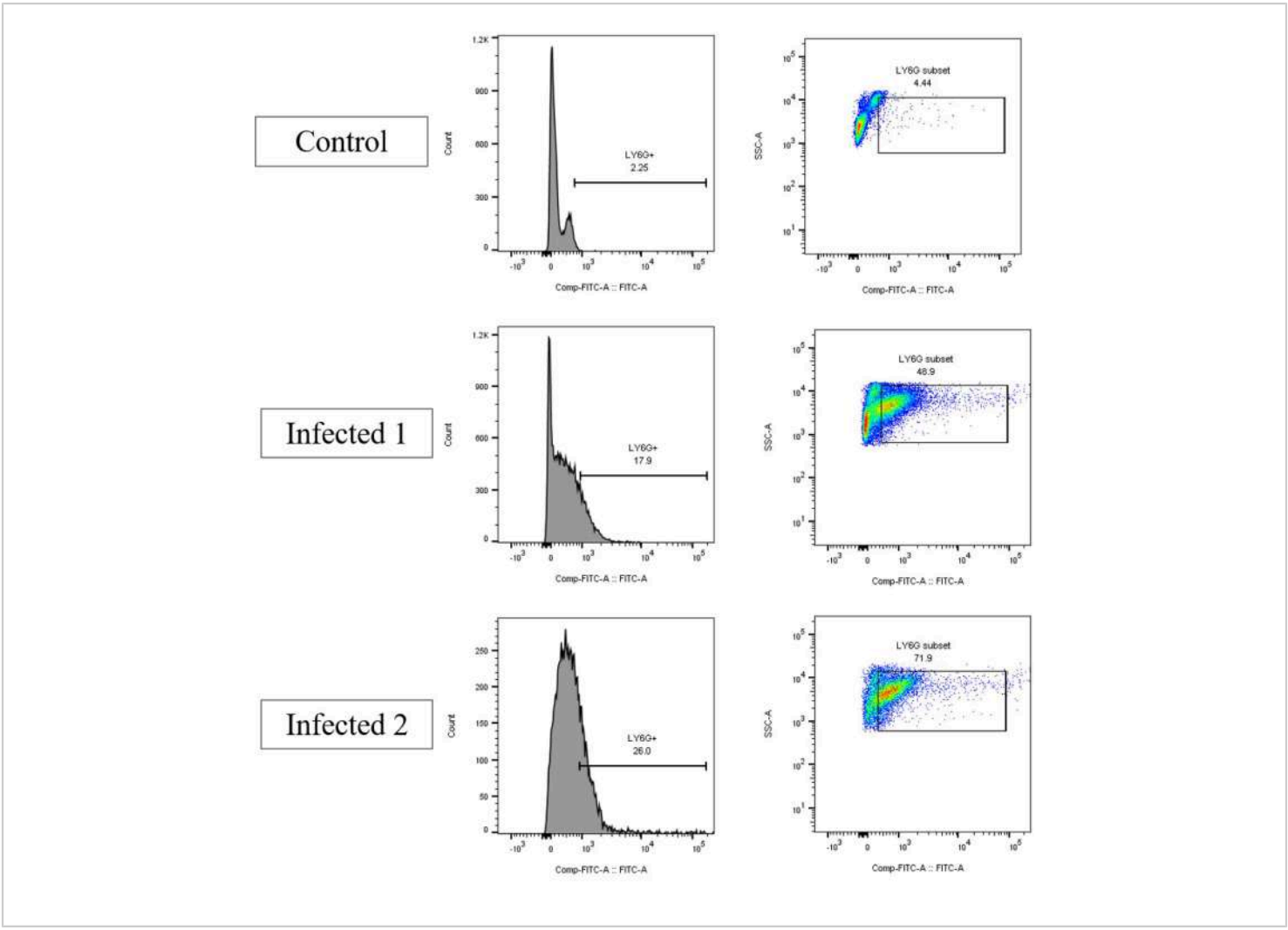

Figure 3: Flow cytometric profiling of neutrophil population in peritoneal lavage fluid. Peritoneal lavage fluid was collected 16 h post infection. The peritoneal cells were stained with FITC-tagged anti-LY6G antibody. Septic mice showed increased infiltration of neutrophils in the peritoneal cavity. Abbreviations: FITC = fluorescein isothiocyanate; LY6G = lymphocyte antigen 6 complex locus G6D; SSC-A = side-scatter area. Please click here to view a larger version of this figure.

Discussion

This article describes a method of inducing a severe form of bacterial sepsis by intraperitoneal injection of *Salmonella* Typhimurium. This model is advantageous over others as *Salmonella* Typhimurium is an intracellular pathogen and, hence, highly pathogenic, mimicking the clinically relevant condition of Gram-negative sepsis. The outcome of peritonitis sepsis in this model is systemic, with 100% mortality within 96 h post infection. Therefore, this model is instrumental in studying the inflammatory and lethal host responses[8] and the effects of therapeutic intervention in attenuating sepsis.

In this model system, the cellular composition of the peritoneal cavity changes dramatically to combat the inoculated pathogen. A large number of $LY6G^+$ neutrophils infiltrate the peritoneal cavity, with a simultaneous decrease in $F4/80^+$

macrophages, resulting in the macrophage disappearance reaction (MDR)[8,10]. Therefore, this model is useful in studying the kinetic changes in immune cell compositions and functions during sepsis, which is still a vastly unexplored area. *Salmonella* Typhimurium systemically infects, resides in, and proliferates in the organs of mice. The serum proinflammatory cytokines such as TNF-α, IL-6, and IFN-γ also increase[8]. A cascade of proinflammatory responses also leads to hemolysis and coagulation of the blood, which becomes visible upon dissection of the infected mice[10,11]. The interplay between the host response to this bacterial burden and the damaging effects of the bacteria leads to disfigured tissue architecture, loss of functions, and tissue necrosis, especially in the liver.

Moreover, previous reports from the laboratory have shown that such effects are modulated by the upregulated expression of nitric oxide synthase 2 (NOS2), which leads to increased reactive oxygen species (ROS) and higher levels of proinflammatory cytokines, leading to an enhanced inflammatory response[8]. This mouse sepsis model is advantageous over others because the induction of sepsis is faster with more lethal effects. It does not require technical expertise to perform the surgery on anesthetized mice, as is the case with the current gold-standard CLP-sepsis mouse model. In the CLP-sepsis model, only a subset of mice develops sepsis, whereas all mice develop sepsis in the model described here.

Moreover, compared to the LPS-induced endotoxemia sepsis model, this model is more clinically relevant for Gram-negative monobacterial sepsis. The model is also useful in understanding the increases in intracellular ROS, proinflammatory cytokine levels, hemolysis, and blood coagulation, all of which happen during sepsis. It is reported that the use of the nitric oxide donor drug DETA-NONOate provides a survival benefit in *Nos2* knockout mice with sepsis using this model[8]. This suggests that this model can be used to identify novel drugs to treat sepsis. Also, this model can be quickly adopted by any laboratory equipped with BSL-2 facilities.

While using this model, precautions must be taken at the level of bacterial cell health and the CFU number to obtain optimal results. One should always use freshly streaked *Salmonella* colonies from SS agar plates. It is also recommended to optimize the process of culture preparation by finding the OD value in the spectrophotometer corresponding to the mentioned CFU.

The disadvantage of using this model is that the effect of sepsis in mice is intensely lethal within 96 h post infection. This limits the study of host immune responses at late time points. It can be overcome by using a more attenuated bacterial strain of *Salmonella* Typhimurium.

There are differences between human patients suffering from sepsis and mice models attempting to mimic human sepsis. For example, patients take longer to develop sepsis and are put on supportive interventions and therapeutics. However, sepsis in mouse models develops much faster, and supportive interventions are not done[4]. However, there are some similarities between sepsis in humans and mice, with patients with sepsis showing higher levels of proinflammatory cytokines, blood coagulation, and hemolysis in clinical settings. All these are mimicked in this mouse model of sepsis. Therefore, some readouts of this model are relevant to clinical scenarios, although a direct correlation may not be advisable.

Disclosures

The authors have no conflicts of interest to disclose.

Acknowledgments

We thank the Central Animal Facility, IISc for supplying us with mice for research. This study was funded by grants to DpN from the Department of Biotechnology and Science and Engineering Research Board, Government of India. The infrastructural support from the DBT-IISc program and DST-FIST grants are greatly acknowledged. We thank all previous and current members of the DpN lab for their support.

References

1. Hotchkiss, R. S. et al. Sepsis and septic shock. *Nature Reviews Disease Primers.* **2** (1), 1-21 (2016).
2. Rudd, K. E. et al. Global, regional, and national sepsis incidence and mortality, 1990-2017: Analysis for the Global Burden of Disease Study. *The Lancet.* **395** (10219), 200-211 (2020).
3. Vincent, J. L. et al. International study of the prevalence and outcomes of infection in intensive care units. *JAMA.* **302** (21), 2323-2329 (2009).
4. Lewis, A. J., Seymour, C. W., Rosengart, M. R. Current murine models of sepsis. *Surgical Infections.* **17** (4), 385-393 (2016).
5. Ta, L., Gosa, L., Nathanson, D. A. Biosafety and biohazards: Understanding biosafety levels and meeting safety requirements of a biobank. *Biobanking.* **1897**, 213-225 (2019).
6. Ray, A., Dittel, D. N. Isolation of Mouse Peritoneal Cavity Cells. *Journal of Visualized Experiments: JoVE.* **35**, 1488 (2010).
7. Liu, X., Quan, N. Immune cell isolation from mouse femur bone marrow. *Bio-protocol.* **5** (20), e1631 (2015).
8. Yadav, S. et al. Nitric oxide synthase 2 enhances the survival of mice during *Salmonella* Typhimurium infection-induced sepsis by increasing reactive oxygen species, inflammatory cytokines and recruitment of neutrophils to the peritoneal cavity. *Free Radical Biology & Medicine.* **116**, 73-87 (2018).
9. Verma, T. et al. Cell-free hemoglobin is a marker of systemic inflammation in mouse models of sepsis: A Raman spectroscopic study. *Analyst.* **146** (12), 4022-4032 (2021).
10. Cassado, A. D. A., Lima, M. R. D., Bortoluci, K. R. Revisiting mouse peritoneal macrophages: Heterogeneity, development, and function. *Frontiers in Immunology.* **6**, 225 (2015).
11. Yadav, S., Verma, T., Chattopadhyay, A., Nandi, D. Factors affecting the pathophysiology of sepsis, an inflammatory disorder: Key roles of oxidative and nitrosative stress. *Indian Journal of Inflammation Research.* **3** (1), RA2 (2019).